AD-A125 832 SEM/TEM FRACTOGRAPHY OF COMPOSITE MATERIALS(U) GENERAL DYNAMICS FORT WORTH TX FORT WORTH DIV 1/2
K M LIECHTI ET AL. SEP 82 AFWAL-TR-82-4085
UNCLASSIFIED F33615-79-C-5121 F/G 11/4 NL

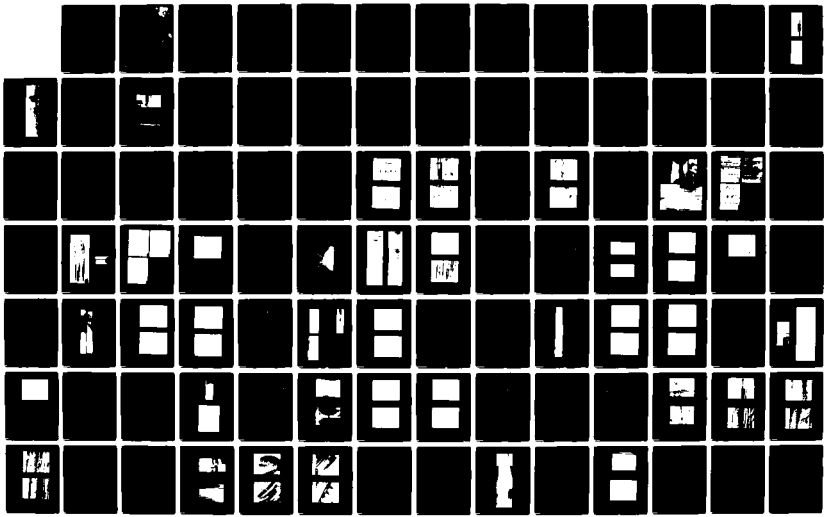

M-2

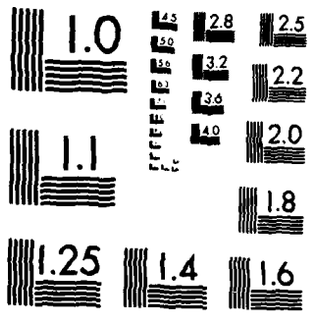


MICROCOPY RESOLUTION TEST CHART
NATIONAL BUREAU OF STANDARDS-1963-A

AD A 125832

AFWAL-TR-82-4085

# SEM/TEM FRACTOGRAPHY OF COMPOSITE MATERIALS

General Dynamics
Fort Worth Division
P.O. Box 748
Fort Worth, Texas 76101

SEPTEMBER 1982

FINAL REPORT FOR PERIOD: October 1979 - March 1982

DTIC
ELECTE
MAR 17 1983
S H D

APPROVED FOR PUBLIC RELEASE; DISTRIBUTION UNLIMITED

MATERIALS LABORATORY
AIR FORCE WRIGHT AERONAUTICAL LABORATORIES
AIR FORCE SYSTEMS COMMAND
WRIGHT-PATTERSON AIR FORCE BASE, OHIO 45433

DTIC FILE COPY

83 03 18 025

## Notice

When Government drawings, specifications, or other data are used for any purpose other than in connection with a definitely related Government procurement operation, the United States Government thereby incurs no responsibility nor any obligation whatsoever; and the fact that the government may have formulated, furnished, or in any way supplied the said drawings, specifications, or other data, is not to be regarded by implication or otherwise as in any manner licensing the holder or any other person or corporation, or conveying any rights or permission to manufacture use, or sell any patented invention that may in any way be related thereto.

This report has been reviewed by the Office of Public Affairs (ASD/PA) and is releasable to the National Technical Information Service (NTIS). At the NTIS, it will be available to the general public, including foreign nations.

This technical report has been reviewed and is approved for publication.

Russell L. Henderson, Sr

RUSSELL L HENERSON, SR
Project Engineer

FOR THE COMMANDER

T D Cooper

T D COOPER, CHIEF
MATERIALS INTEGRITY BRANCH
SYSTEMS SUPPORT DIVISION

"If your address has changed, if you wish to be removed from our mailing list, or if the addressee is no longer employed by your organization please notify AFWAL/MLSA, W-PAFB, OH 45433 to help us maintain a current mailing list".

Copies of this report should not be returned unless return is required by security considerations, contractual obligations, or notice on a specific document.

Unclassified

SECURITY CLASSIFICATION OF THIS PAGE (When Data Entered)

| REPORT DOCUMENTATION PAGE | | READ INSTRUCTIONS BEFORE COMPLETING FORM |
|---|---|---|
| 1. REPORT NUMBER<br>AFWAL-TR-82-4085 | 2. GOVT ACCESSION NO.<br>AD-A125832 | 3. RECIPIENT'S CATALOG NUMBER<br>FZM 7078 |
| 4. TITLE (and Subtitle)<br>SEM/TEM FRACTOGRAPHY OF COMPOSITE MATERIALS | | 5. TYPE OF REPORT & PERIOD COVERED<br>Technical - Final<br>October 1979-March 1982 |
| | | 6. PERFORMING ORG. REPORT NUMBER |
| 7. AUTHOR(s)<br>K. M. Liechti, J. E. Masters, D. A. Ulman<br>M. W. Lehman | | 8. CONTRACT OR GRANT NUMBER(s)<br>F33615-79-C-5121 |
| 9. PERFORMING ORGANIZATION NAME AND ADDRESS<br>General Dynamics/Fort Worth Division<br>P. O. Box 748<br>Fort Worth, Texas | | 10. PROGRAM ELEMENT, PROJECT, TASK AREA & WORK UNIT NUMBERS<br>24180715 |
| 11. CONTROLLING OFFICE NAME AND ADDRESS<br>Materials Laboratory (AFWAL/MLSA)<br>Air Force Wright Aeronautical Laboratories<br>AFSC, WPAFB, OH 45433 | | 12. REPORT DATE<br>September 1982 |
| | | 13. NUMBER OF PAGES<br>100 |
| 14. MONITORING AGENCY NAME & ADDRESS(if different from Controlling Office) | | 15. SECURITY CLASS. (of this report)<br>Unclassified |
| | | 15a. DECLASSIFICATION/DOWNGRADING SCHEDULE |

16. DISTRIBUTION STATEMENT (of this Report)

Approved for public release; distribution unlimited.

17. DISTRIBUTION STATEMENT (of the abstract entered in Block 20, if different from Report)

18. SUPPLEMENTARY NOTES

19. KEY WORDS (Continue on reverse side if necessary and identify by block number)

Composite Materials, Graphite Epoxy, Fracture Mechanics, Fractography, SEM/TEM

20. ABSTRACT (Continue on reverse side if necessary and identify by block number)

Basic unidirectional laminae and a simple quasi-isotropic laminate were mechanically tested to failure under tensile and compressive loads. A fractographic investigation of these specimens and specimens made available from Arcan shear tests, Mode I and Mode II fracture tests, three-point bend tests and (continued)

DD FORM 1 JAN 73 1473 EDITION OF 1 NOV 65 IS OBSOLETE

Unclassified

SECURITY CLASSIFICATION OF THIS PAGE (When Data Entered)

20. Abstract (Continued)

low velocity impact tests was conducted. Procedures for conducting these analyses are defined and emphasize the need for considering information available from macroscopic as well as microscopic considerations. Fractographic features in the matrix material were found to provide more information on the failure processes than fractographic features in the fibers. The brittle nature of the matrix material at room temperature resulted in fracture planes which were perpendicular to the local maximum principal stress direction.

## FOREWORD

This final technical report describes the work performed under Contract No. F33615-79-C-5121 from October 1979 to March 1982. The program was sponsored by the Materials Laboratory, Air Force Wright Aeronautical Laboratories, Air Force Systems Command, Wright-Patterson Air Force Base, OH 45433, with Mr. R. L. Henderson of AFWAL/MLSA as Project Engineer.

Dr. K. M. Liechti, the General Dynamics Fort Worth Division Program Manager, has been responsible for the compilation of this document. The work of his predecessor, Dr. J. E. Masters, who made the major contribution is therefore gratefully acknowledged. Messrs. M. W. Lehman and W. S. Margolis were also responsible for the fractography task and D. A. Ulman assisted in the testing.

Accession For
NTIS GRA&I ☑
DTIC TAB ☐
Unannounced ☐
Justification
By
Distribution/
Availability Codes
Dist | Avail and/or Special
A

DTIC COPY INSPECTED 2

TABLE OF CONTENTS


| Section | | Page |
|---|---|---|
| 1. | INTRODUCTION | 1 |
| | 1.1 Literature Review | 7 |
| 2. | GUIDE TO PROCEDURES | 10 |
| 3. | CONFIGURATION AND TESTING OF SPECIMENS | 12 |
| | 3.1 Material Selection | 12 |
| | 3.2 Specimen Geometries and Loading | 12 |
| 4. | FRACTOGRAPHIC RESULTS | 22 |
| | 4.1 Shear Specimens | 26 |
| | 4.2 Mode I Fracture Specimens | 40 |
| | 4.3 Mode II Fracture Specimens | 45 |
| | 4.4 Three Point Bend Specimens | 45 |
| | 4.5 Tension Specimens | 53 |
| | 4.5.1 $90^{\circ}$ Laminae | 53 |
| | 4.5.2 $0^{\circ}$ Laminae | 61 |
| | 4.5.3 $\pm 45^{\circ}$ Laminae | 61 |
| | 4.6 Compression Specimens | 69 |
| | 4.6.1 $90^{\circ}$ Laminae | 69 |
| | 4.6.2 $\pm 45^{\circ}$ Laminae | 75 |
| | 4.6.3 Quasi Isotropic Laminae | 80 |
| | 4.7 Impact Damage Specimen | 80 |

TABLE OF CONTENTS (Continued)


| Section | | Page |
|---|---|---|
| 5. | CONCLUDING REMARKS | 86 |
| | REFERENCES | 88 |
| | APPENDIX | 91 |

## LIST OF FIGURES


| Number | Title | Page |
|---|---|---|
| 1. | Photomicrograph of the Edge of a $[0/\pm45/90]_S$ T300/5208 Laminate | 3 |
| 2. | Delamination Development in $[0/\pm45/90]_S$ Laminate | 3 |
| 3. | DIB Enhanced X-Ray Radiograph of $[0/\pm45/90]_S$ Laminate | 4 |
| 4. | Macroscopic Fractographs of Typical $[0/\pm45/90]_{2S}$ Laminate | 6 |
| 5. | Coupon Geometry for Tensile Testing of $0^\circ$ Lamina | 14 |
| 6. | Coupon Geometry for Tensile and Tension-Tension Fatigue Testing of $90^\circ$ and $\pm45^\circ$ laminae and $[0/\pm45/90]_{2S}$ Laminates | 14 |
| 7. | Coupon Geometry for Monotonic Compression and Tension-Compression Fatigue Testing of $0^\circ$, $90^\circ$ and $\pm45^\circ$ Laminae and $[0/\pm45/90]_{2S}$ Laminates | 15 |
| 8. | Arcan Shear Specimen Geometry | 16 |
| 9. | Mode I Fracture Mechanics Specimen | 18 |
| 10. | Mode II Fracture Mechanics Specimen | 19 |
| 11. | Three-Point Bend Test Specimens | 20 |
| 12. | Low Velocity Impact Test Specimens | 21 |
| 13. | Photomicrographs of Hackle Pattern | 24 |
| 14. | River Pattern in Resin Pocket in Mode I Specimen | 24 |
| 15. | River Pattern in Resin Material Between Fibers in Mode I Specimen | 25 |
| 16. | Photomicrograph of Feather Pattern in Mode I Specimen | 25 |

LIST OF FIGURES (Continued)


| Number | Title | Page |
|---|---|---|
| 17. | Photomicrograph of Feather Pattern in Mode II Specimen | 27 |
| 18. | Typical Fiber Fracture Surfaces | 27 |
| 19. | Arcan Shear ($G_{12}$) | 28 |
| 20. | Arcan Shear ($G_{31}$) | 32 |
| 21. | Arcan Shear ($G_{23}$) | 36 |
| 22 | Mode I Fracture | 41 |
| 23. | Mode II Fracture | 46 |
| 24. | $0^{\circ}$ Flexture (1) | 50 |
| 25. | $0^{\circ}$ Flexture (2) | 54 |
| 26. | $90^{\circ}$ Tension | 58 |
| 27. | $0^{\circ}$ Tension | 62 |
| 28. | ±45 Tension | 64 |
| 29. | Schematic of Transverse Cracks in $\pm 45^{\circ}$ Specimen | 68 |
| 30. | $90^{\circ}$ Compression | 70 |
| 31. | $\pm 45^{\circ}$ Compression | 76 |
| 32. | Quasi-Isotropic Compression | 81 |
| 33. | Transverse Impact | 83 |
| 34. | Schematic of Formation of Cleavage and Hackle Features | 86 |

# 1. INTRODUCTION

The introduction to Volume 9 of the American Society for Metals' Metals Handbook(1) states: "The term 'fractography' was coined in 1944 to describe the science of studying fracture surfaces, although fractures and fracture surfaces had been examined and studied for centuries as part of the art of metallurgy. The two chief metallurgical benefits of fractography are: (a) it is an important tool in failure analysis, and (b) it provides new information regarding the micromechanics of fracture and the internal structural features of the solid state."

As this basic definition implies, the science of fractography has been developed into a tool which can be applied to all phases of metallurgical investigation. Obviously there are parallel applications of fractography to composite materials. As a production tool, microscopy could be applied to assess the quality of incoming material once key accept/reject features have been identified. In the laboratory, fractography can be used to define failure mechanisms in control specimens. This information could be applied to material selection and optimization. It would also provide the insight required to develop mechanistic analyses. Finally, since production components in both military and commercial aircraft now utilize graphite/epoxy composites, a thorough knowledge of the material's fracture behavior and the component's failure modes is required to determine air-worthiness and to investigate in-service component failure.

Unfortunately, fractography has not kept pace with the rapid advancement of composite materials from a laboratory curiosity in the 1960's to production components in the 1980's. An obvious approach when developing fractographic data for composite materials is to examine the failure surface for features which have been identified in the fractography of metals; i.e., look for parallels in the two systems. The hope here is to apply directly the knowledge gained over the years in the fractography of metals to the fractography of composites. While some features (e.g., cleavage planes) are common to the two materials and the metallographic observations provide insight, solely adopting this approach will prove to be very frustrating since the two systems are fundamentally different.

In defining composite materials, R. M. Jones (2) states, "The word composite material signifies that two or more materials are combined on a macroscopic scale to form a

useful material. The advantage of composites is that they exhibit the best qualities of their constituents and often some qualities that neither constituent, by itself, possesses." Therefore, composites are inhomogeneous on a macroscopic scale. Continuous fiber-laminated composites are further complicated because they are anisotropic. These factors limit the applicability of several fundamental precepts developed for "traditional" engineering materials.

Due to the anisotropy of the individual lamina, complex internal stress states develop when lamina are cured to form a laminate and load is applied to that laminate. These stress states include both in-plane ($\sigma_x$, $\sigma_y$, and $\tau_{xy}$) and out-of-plane (interlaminar normal $\sigma_z$, and shear $\tau_{xz}$, $\tau_{xz}$) stresses. The interlaminar normal and shear stresses are a function of the laminate stacking sequence. Small changes in the stacking sequence can significantly alter these stresses. For example, a $[0/90/\pm45]_S$ laminae will develop compressive $\sigma_z$ stresses under applied axial tensile load while a $[0/\pm45/90]_S$ laminate will develop tensile $\sigma_z$ stresses. This stress reversal alters the pattern of damage development in the laminates and affects the final failure events. It is therefore imperative that a thorough stress analysis be performed when investigating laminate response.

The presence of these complex stress states results in the development of damage modes not normally encountered in metals. For example, Fig. 1 is a photomicrograph of the edge of a $[0/\pm45/90]_S$ T300/5208 graphite epoxy laminate loaded in axial tension. In addition to tensile in-plane ($\sigma_x$) stresses, the laminate also develops tensile interlaminar normal ($\sigma_z$) stresses under this type of loading. As the figure demonstrates, transverse cracks (matrix cracks in off-axis plies extending across the specimen width parallel to the fiber direction) developed in both the interior 90° lamina and in each of the adjacent -45° lamina. The photomicrograph also illustrates that longitudinal cracks (matrix cracks parallel to the applied load, extending along the specimen length) developed from the transverse cracks in the 90° lamina. These cracks developed at several locations and, with increased loading, propagated axially along the specimen length. Eventually they all linked together forming a continuous edge delamination (Fig. 2) which spanned the entire specimen length. At even higher loads, this delamination propagated into the specimen interior.

Figure 3 is a diiodobutate (DIB) enhanced X-ray radiograph of a $[0/\pm45/90]_S$ laminate that has been subjected to 1 million cycles of tension-tension fatigue (R=.1,

Figure 1 Photomicrograph of the Edge of a $[0/\pm45/90]_S$ Laminate

Figure 2 Delamination Development in $[0/\pm45/90]_S$ Laminate

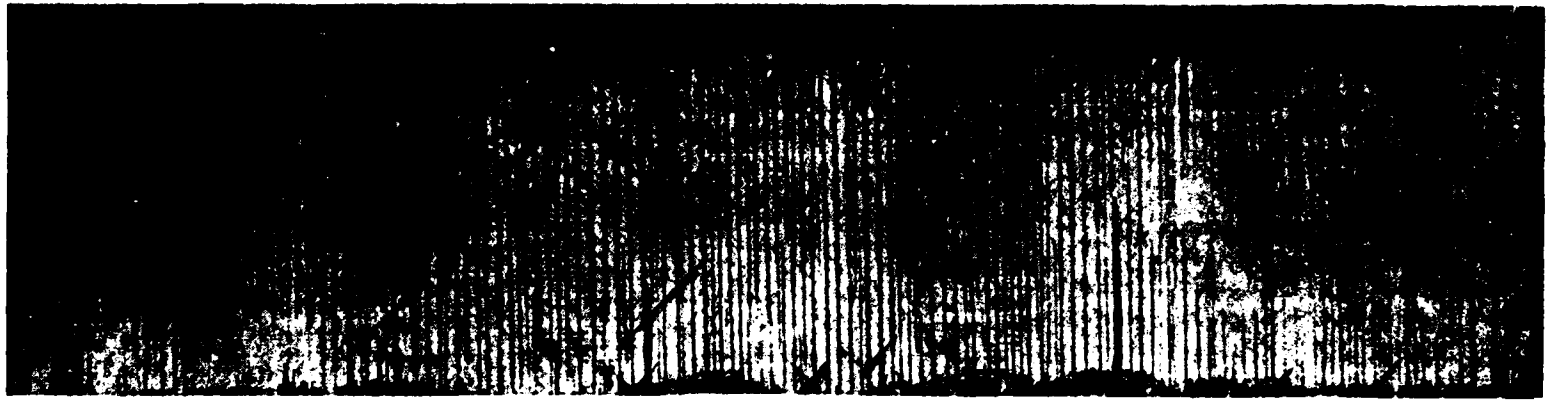

Figure 3 DIB Enhanced X-Ray Radiograph of $[0/\pm45/90]_S$ Laminate

f=15Hz). The dark horizontal and 45° lines which cross-hatch the specimen are transverse cracks which developed during the cycling. The dark areas at either specimen edge are delaminations which grew into the specimen interior. The figure illustrates the degree of damage which can develop in the material prior to failure. In this type of specimen, damage is distributed uniformly over the specimen length. Final failure will occur at the weakest cross-section which may be located anywhere along the specimen length. If stress raisers are introduced into the specimen (e.g., open holes), the final failure site will then be defined. Experimental evidence indicates, however, that again final failure will be preceded by a series of separate events including matrix cracking, fiber breakage and delamination.

The ultimate failure of a composite laminate is a high energy event. The magnitude of energy released is directly proportional to the number of 0° lamina present. The combination of this high energy release and the large amount of pre-failure damage produces a highly fragmented failure surface (Fig. 4) making comprehensive fractography quite difficult.

In summary, the analysis of composite material failure surfaces is complicated by the nature of the material. Due to the macroscopic material inhomogeneity, each fiber-matrix interface serves as a possible matrix crack initiation site. The anisotropic nature of the individual lamina results in complex internal stress states which further complicate the failure processes. The fracture of a composite component is therefore quite different from the fracture of a metallic component. There is no single self-similar crack but a damage zone in which matrix cracking, fiber breakage and delamination combine to yield component failure. In the examples presented above, the damage zone extended over the entire specimen.

As stated earlier, the fractography of complicated structural laminates featuring numerous off-axis lamina will ultimately need to be addressed. These laminates contain intricate internal stress distributions which result in complex failure modes. The basic premise of the work presented here is that the problem can be separated into several elemental problems. That is, fractographic features indicative of fundamental failure modes can be identified and used to interpret the failure of more advanced laminates.

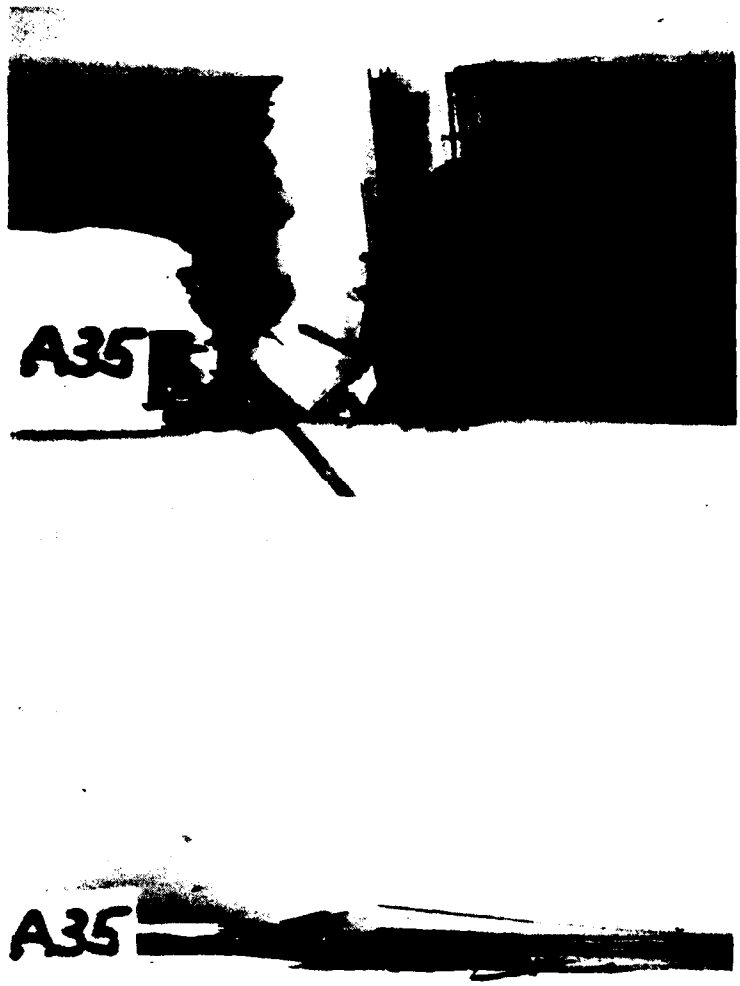


Figure 4 Macroscopic Fractographs of Typical $[0/\pm45/90]_{2S}$ Failure Surface , 2X

## 1.1 Literature Review

A review of recent literature has shown that several researchers have performed fractographic analyses of high modulus graphite/epoxy material systems. Miller and Wingert (3) studied the fracture surface morphologies of graphite/epoxy composites to investigate the influences of load history, material configuration, temperature and moisture. Unidirectional 0° lamina fabricated from prepreg tape were loaded in axial tension. Short beam shear tests were conducted on specimens fabricated from woven fabric. In similar studies, Clements (4,5) performed tension tests on $[0]_8$ T300/5208 lamina to determine the influence of moisture (0% and 2% content) and temperature (25°C and 96°C) on failure strength. The fractographic results of Clements' studies include the definition of high energy and low energy surface morphology for 0° lamina.

The off-axis tensile response of unidirectional lamina has also been the subject of several investigations. Chamis and Sinclair (6,7) studied the failure surfaces of unidirectional Modmor II/4617 lamina. Several loading angles were investigated: 0, 5, 10, 15, 30, 45, 60, 75 and 90°. (Angles are measured from the fiber axial direction). Fracture modes associated with approximate load angle ranges were identified. The fracture modes identified were: (1) longitudinal tensile fracture - characterized by irregular, tiered failure surfaces dominated by fiber fracture and fiber pullout, (2) intralaminar shear stress fracture - characterized by regular or level failure surfaces which contain extensive matrix lacerations, (3) transverse tensile fracture - again characterized by regular or level failure surfaces but containing extensive matrix cleavage features and, (4) mixed mode (transverse tensile and intralaminar shear) - characterized by level fracture surfaces containing areas of both resin cleavage and resin laceration features. Awerbuch and Hahn (8) studied the off-axis tensile static and fatigue behavior of unidirectional AS/3501-5 graphite/epoxy lamina in an effort to characterize matrix-interface controlled failure. They also investigated several load angles: 0, 10, 20, 30, 45, 60, and 90 deg. Among the conclusions of this work, the authors noted that fracture surfaces included a combination of several independent failure modes, such as fiber fracture, matrix serration (shear failure), matrix cleavage and matrix/interface cracking parallel to the fibers. They also noted variations in matrix failure characteristics with off-axis angle, stating that matrix serrations increase with longitudinal shear stress. In the absence of shear stress, a cleavage type of failure prevails.

Morris (9) examined the fracture surfaces of 40 ply thick 0°, 90° and ±45° T300/5208 edge notched tensile specimens. He observed that the surfaces consisted of graphite fiber and epoxy components. Morris noted that "hackles" (raised epoxy platelets identified as lacerations and serrations by Chamis and Awerbuch, respectively) were the most commonly exhibited epoxy matrix components. The hackle platelets lie between adjacent parallel graphite fibers and are oriented approximately normal to the fiber axes. Individual hackles are flake-like in appearance. They overlap one another in a manner similar to shingles on a roof. Hackles were present on both mating surfaces of the specimens studied and had consistent tilt inclination directions over each surface. However, the hackle tilt direction was reversed on the mating surface pointing in the opposite direction.

Fatigue of graphite/epoxy composites is also a major area of study. As mentioned earlier, Awerbuch and Hahn examined the fatigue behavior of unidirectional lamina loaded in off-axis tension-tension fatigue. They noted that specimens failed in a "sudden-death" mode, that is, specimen strength decreased rapidly immediately before failure. This behavior was attributed to rapid crack growth immediately before fracture. Adams (10,11) investigated the failure surfaces of AS/3501-6 specimens subjected to compression and compression fatigue. Fiber microbuckling was observed as a common failure mode in both static and fatigue specimens containing 0° lamina. Adams also noted that fiber-matrix debond within a ply and debonding at lamina interfaces were also primary failure modes in specimens subjected to compression loads. Morris and Hetter (12) studied AS/3501-6 laminates in tension-compression fatigue. Their test coupons had center holes but fasteners were not applied. Patterns of arrest marks (striations) associated with tension-compression fatigue crack propagation were located in some specimens.

Adams also investigated impact damage in graphite/epoxy and hybrid composite materials (13,14). The all-graphite control specimens investigated in these studies consisted of Modmor II graphite fibers impregnated with Narmco 1004 epoxy resin. Fracture surfaces of static flexure and charpy impact specimens were examined in detail on the scanning electron microscope. Observed similarities and differences between fracture characteristics observed in these surfaces are noted. Morris (9) studied low-velocity impact phenomena in quasi-isotropic graphite/epoxy laminates bonded to phenolic honeycomb core material. He observed that hackles were again the predominant epoxy matrix feature.

Finally, Purslow (15) reported results of a detailed study of graphite/epoxy lamina and laminates subjected to a variety of load conditions including: axial tension, off-axis tension, shear, axial compression and flexure.

Section 2, which follows this introduction, is intended as a basic guide to the procedures involved in a fractographic investigation of laminated composite materials. It will also discuss the specimen preparation and procedures involved in the use of the Scanning Electron Microscope. Section 3 defines the material systems, the test specimen geometries and the test procedures. The fractographic results that were obtained for the various specimens will be presented in Section 4. Finally, the results are discussed and summarized in Section 5.

## 2.0 GUIDE TO PROCEDURES

In conducting a fractographic analysis, particularly on a microscopic scale, a large amount of information can accumulate very quickly. It is therefore necessary to carefully plan and record the steps involved in any analysis in order to ensure proper interpretation and avoid confusion. A "Composite Material Fractography Record" is included in the Appendix as an example of the procedures involved.

The first step is to view the subject part and its surroundings on the macroscopic scale, noting the locations of stress concentrations such as holes and ply terminations. The load and environmental histories to which the part has been subject should then be determined. The foregoing information, in conjunction with any available NDE records, then provides a basis for determining all the possible origins and paths of fracture. The importance of these macroscopic considerations in understanding the failure of the specimens examined in this study and composites in general cannot be overemphasized.

These preparations allow for the formation of a sectioning plan in which the most likely fracture paths contributing to the final failure are followed. Although graphite epoxy can be observed under a SEM without first coating the surface that is being observed, the noise to signal ratio is rather high and interpretation of the image can be difficult. If the surface under observation is coated, then a balance must be struck between losing topographic information due to too thick a coating and the disadvantages of not coating that have just been noted. In the specimens that were examined in this study, the Gold/Paladium coating was vacuum deposited to an average thickness of 300 Angstroms.

The presence of initial defects such as voids, porosity and granulation can be identified at relatively low magnifications. This information, in conjunction with the macroscopic considerations alluded to earlier is generally sufficient to locate the sources of failure. Further increasing magnification in these areas serves to identify fractographic features that indicate the direction of crack growth. It is at these higher magnifications that careful record keeping can greatly facilitate the determination of failure of a part. In addition, the magnification, specimen orientation and image enhancement features such as frequency and Gamma amplification, backscattered electron images and

accelerating voltage should be noted so that communication between investigators can be standardized.

The discussion of the specimens and their testing and the fractographic results that now follows, serves to identify the features that provide the clues that are used to determine the causes of failure in composite materials.

## 3. CONFIGURATION AND TESTING OF SPECIMENS

### 3.1 Material Selection

Two basic material systems were investigated in this study; namely, T300/5208 (Narmco) and AS1/3501-6 (Hercules). Both systems cure at 350°F and feature unmodified epoxy matrix resins (i.e., they contain no elastomeric additives which can precipitate out to form a dispersion of soft inclusions in the rigid matrix material). Although the exact composition of the resins is proprietary to the two manufacturers, qualitative characterizations do appear in the literature. Carpenter (16) used U.V. and IR chromatograms of 3501-6 resin to identify three epoxides and a curing agent, DDS. Similarly, Kibler (17) applied liquid chromatography to 5208 resin and noted the presence of a major epoxy, a minor epoxide and a curing agent DDS.

The chemical characteristics of T300/5208 and AS1/3502 have also been compared (Ref. 23) and found to be similar. A number of CRAD and IRAD projects have determined that the mechanical properties are also equivalent. Furthermore, documentation from Hercules indicates that AS1/3501-6 and AS1/3502 have mechanical properties that are closely equivalent. The mechanical properties of AS1/3501-6 and T300/5208, both used in this study, must therefore be equivalent. In anticipation of the fractographic results to be discussed later, the association is close at hand that the fracture morphologies of the two materials will also be equivalent.

Since the matrix materials of the composites studied here are polymeric, they are potentially viscoelastic. Kibler (Ref. 17) found that the material properties of both T300/5208 and AS1/3502 were time, temperature and moisture dependent. Environmental conditions can also be expected to affect the fracture morphology. For example, Miller and Wingert (Ref. 3) found that elevated temperature and moisture resulted in increased fiber pullout in graphite/epoxy systems. While the importance of environmental conditions has been noted here, fractographic investigations were made of specimens which were tested under the environmental condition of room temperature, dry.

### 3.2 Specimen Geometries and Loading

The key to interpreting the failure of complex laminates (i.e., those featuring lamina with a variety of fiber

orientations and therefore containing complex internal stress distributions) is to isolate and identify the basic mechanisms of crack growth in basic lamina configurations which are subject to basic and well-defined stress distributions. The philosophy of this program has therefore been to examine as many experimentally attainable combinations of crack growth modes in unidirectional laminates as possible. Eight basic specimen geometries (Figures 5-12) have therefore been investigated; some of the geometries were used for more than one orientation of unidirectional plies. These geometries are now discussed in more detail.

Two geometries were used for monotonic tensile and tension-tension fatigue testing. The first, used only in tensile testing of 0° laminae, is shown in Figure 5. The specimen was 9 inches long, 0.5 inches wide and 6 plies thick. The second geometry (Figure 6) had the same length, but was wider (1 inch) and thicker (16 plies), and was used for tensile testing of 90° and ±45° laminae and tensile and tension-tension fatigue testing of $[0/\pm45/90]_{2S}$ laminates. The 0° (and loading) direction is defined in both figures.

Compression testing required shorter and thicker specimens to ensure that relatively high strains could be introduced prior to buckling. The geometry for the 0°, 90° and +45° laminae under monotonic compression and a $[0/\pm45/90]_{2S}$ laminate under monotonic compression and tension-compression fatigue tests is shown in Figure 7. The unsupported length of the seven inch long, 1 inch wide, 48 ply thick specimens was 4 inches. The 0° direction was again axial.

All of the aforementioned specimens were fabricated and tested specifically for this program. Five other geometries were available from other programs being conducted at GD/FWD; namely, Arcan shear specimens, Mode I and Mode II fracture specimens, three-point bend specimens and, finally, a specimen used in low velocity impact studies.

The Arcan or "Butterfly" specimen, developed by Arcan et al., was used at General Dynamics to determine the shear stiffness and failing stress and strain of T300/5208 (Ref. 18). The specimen dimensions and direction of applied load are shown in Figure 8 . Specimens were machined from a thick, unidirectional laminate so as to obtain values of $G_{12}$, $G_{23}$ and $G_{31}$ as defined in Figure 8 . The design and loading of the specimens is such that a condition of pure shear exists in the center of the notched region.

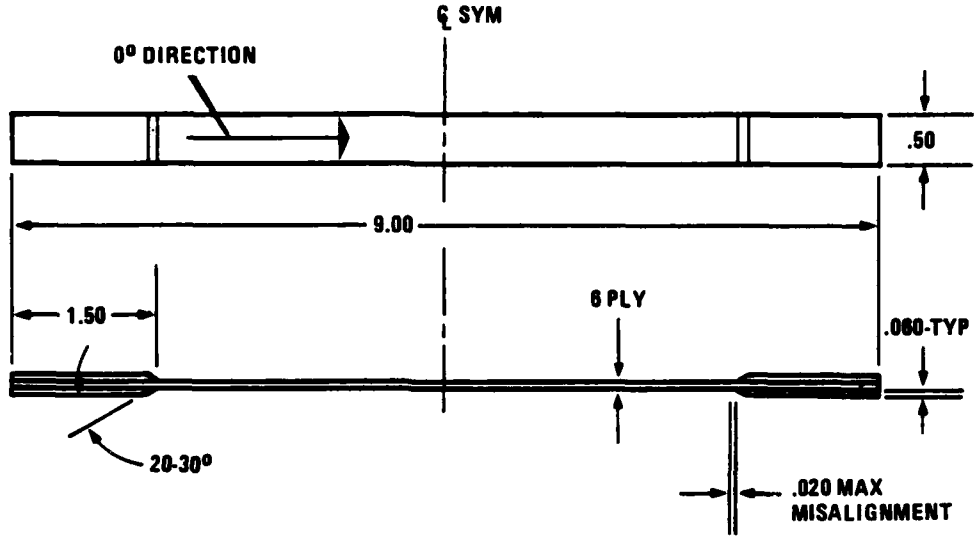


Figure 5 Coupon Geometry For Tensile Testing of 0° Laminae

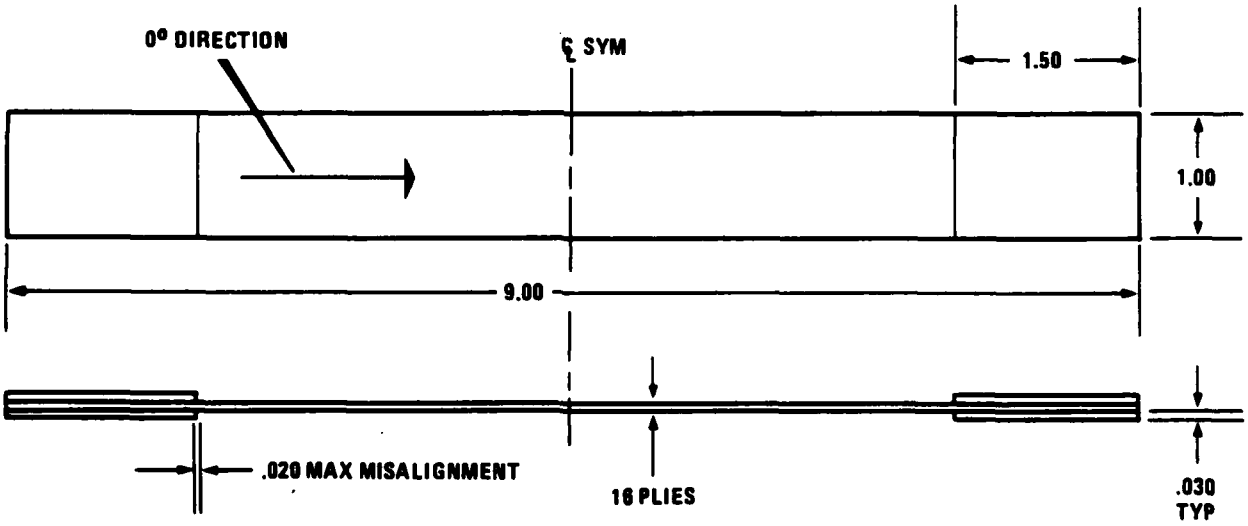


**Figure 6 Coupon Geometry for Tensile and Tension-Tension Fatigue Testing of 90° and ±45° Laminae and $[0/\pm45/90]_{2S}$ Laminates**

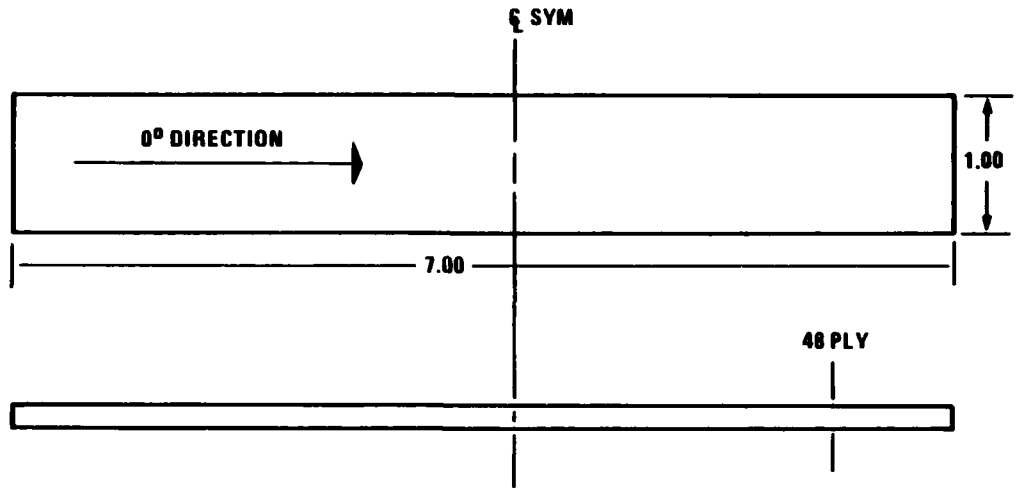


Figure 7 Coupon Geometry for Monotonic Compression and Tension-Compression Fatigue Testing of 0°, 90°, and ±45° Laminae and $[0/\pm45/90]_{2S}$ Laminates

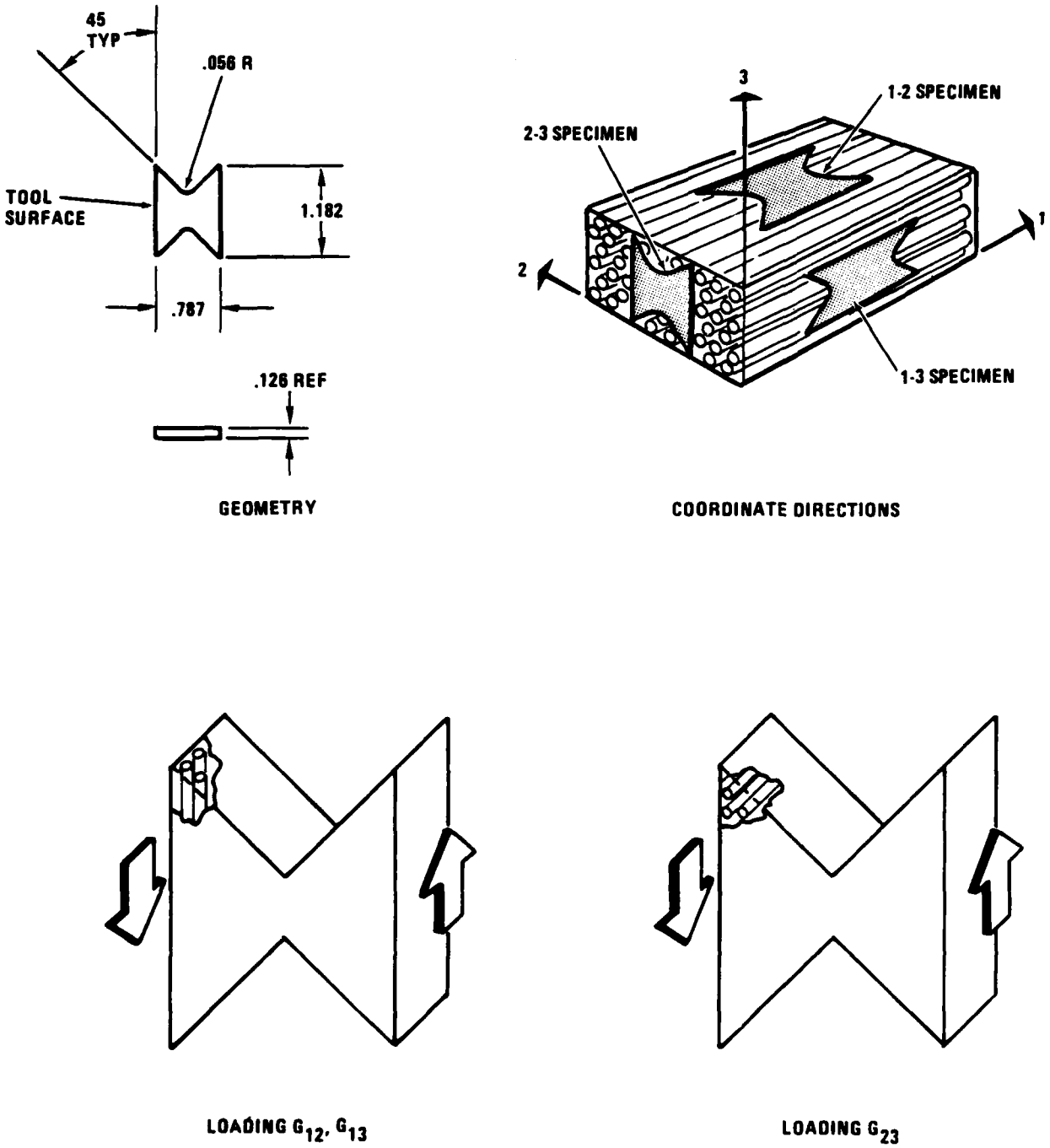


Figure 8 ARCAN Shear Specimen

Wilkins modeled delamination growth in graphite epoxy composite materials using fracture mechanics concepts (Ref. 19). Measurements were made of static and fatigue fracture properties in the opening and forward shear modes of fracture (Mode I and Mode II, respectively). The geometries of the Mode I and Mode II specimens and schematics of the loadings are shown in Figures 9 and 10, respectively. In these tests, single, self-similar cracks were propagated between adjacent 0° laminae. A thin strip of Kapton film was cured into the laminates to control the location of the crack initiation site. Calculations of strain energy release rates were made from compliance and crack length measurements.

Three-point bend tests are routinely conducted at General Dynamics' Fort Worth Division to determine the 0° flexural modulus in the quality assurance of incoming graphite epoxy prepreg material (Ref. 20). The specimen geometry and directions of fibers and applied load are shown in Figure 11.

The geometry and loading of the low velocity impact specimens made available for fractographic examination are shown in Figure 12. The 6 inch square plates were 28 plies thick and were made of T300/5208. They were supported over a 5 inch square area and struck by a 0.625 inch hemisphere in a standard "instrumented impact" test (Ref. 21,22).

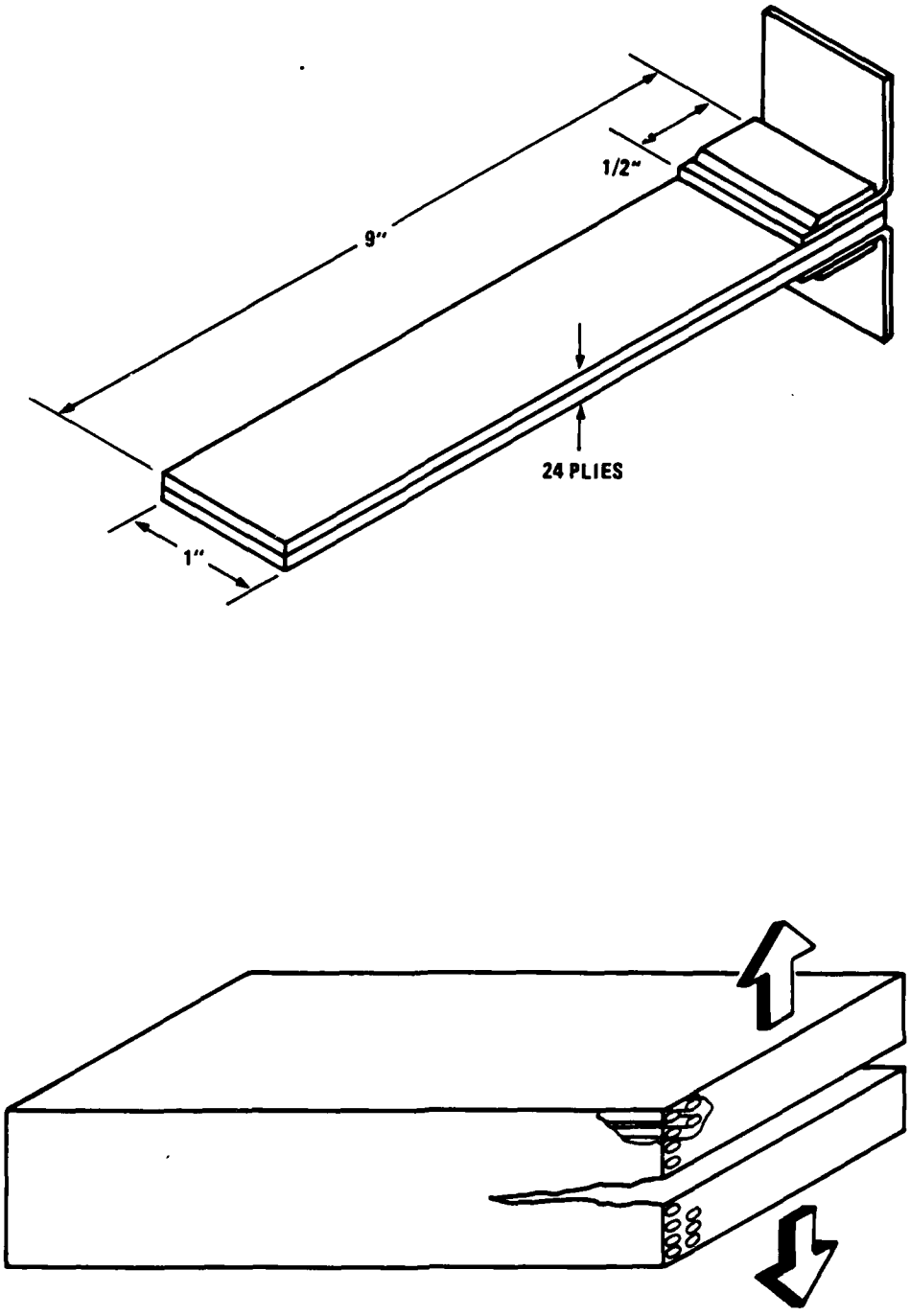


**Figure 9 Mode I Fracture Mechanics Specimen**

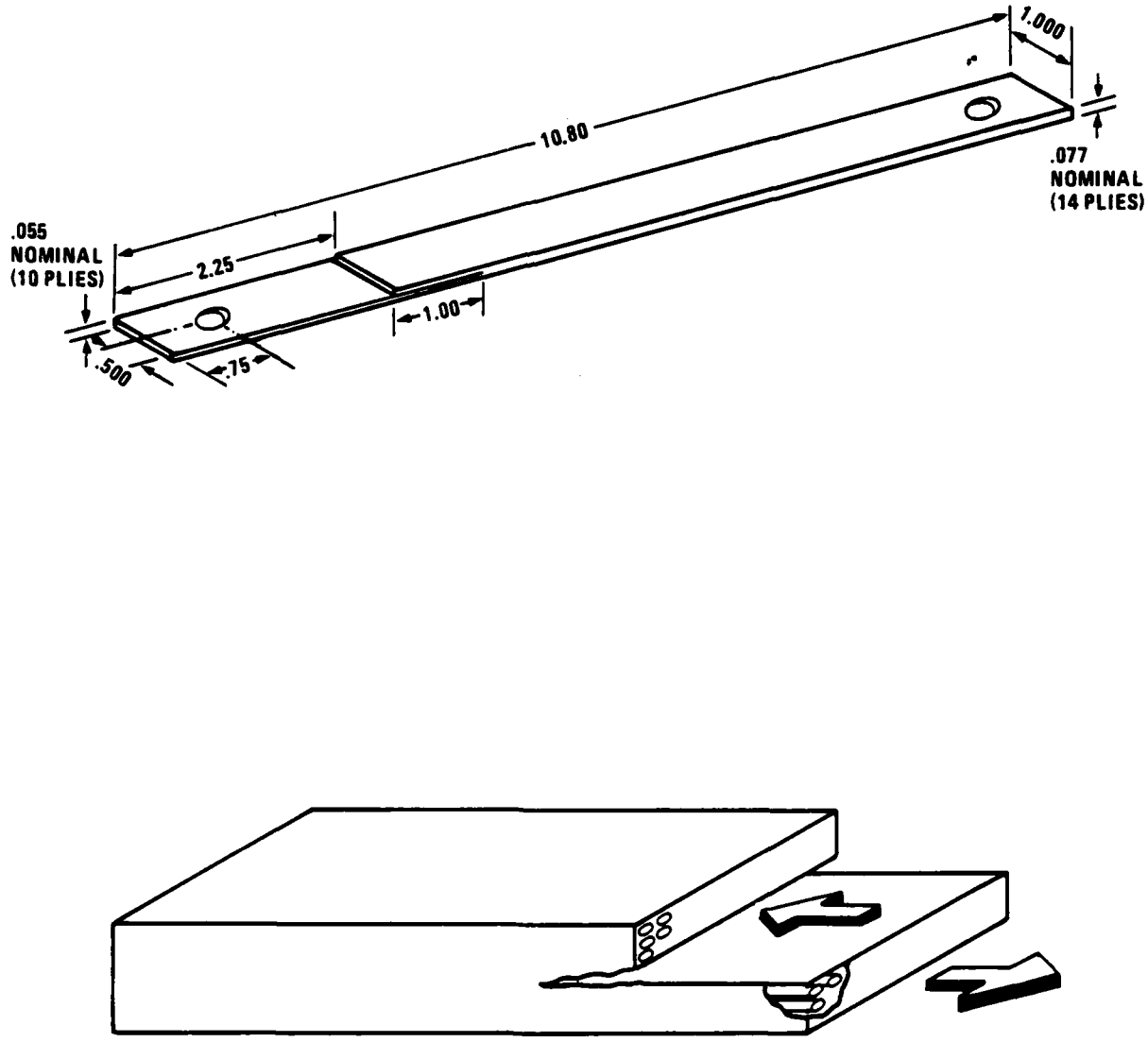


Figure 10 Mode II Fracture Mechanics Specimen

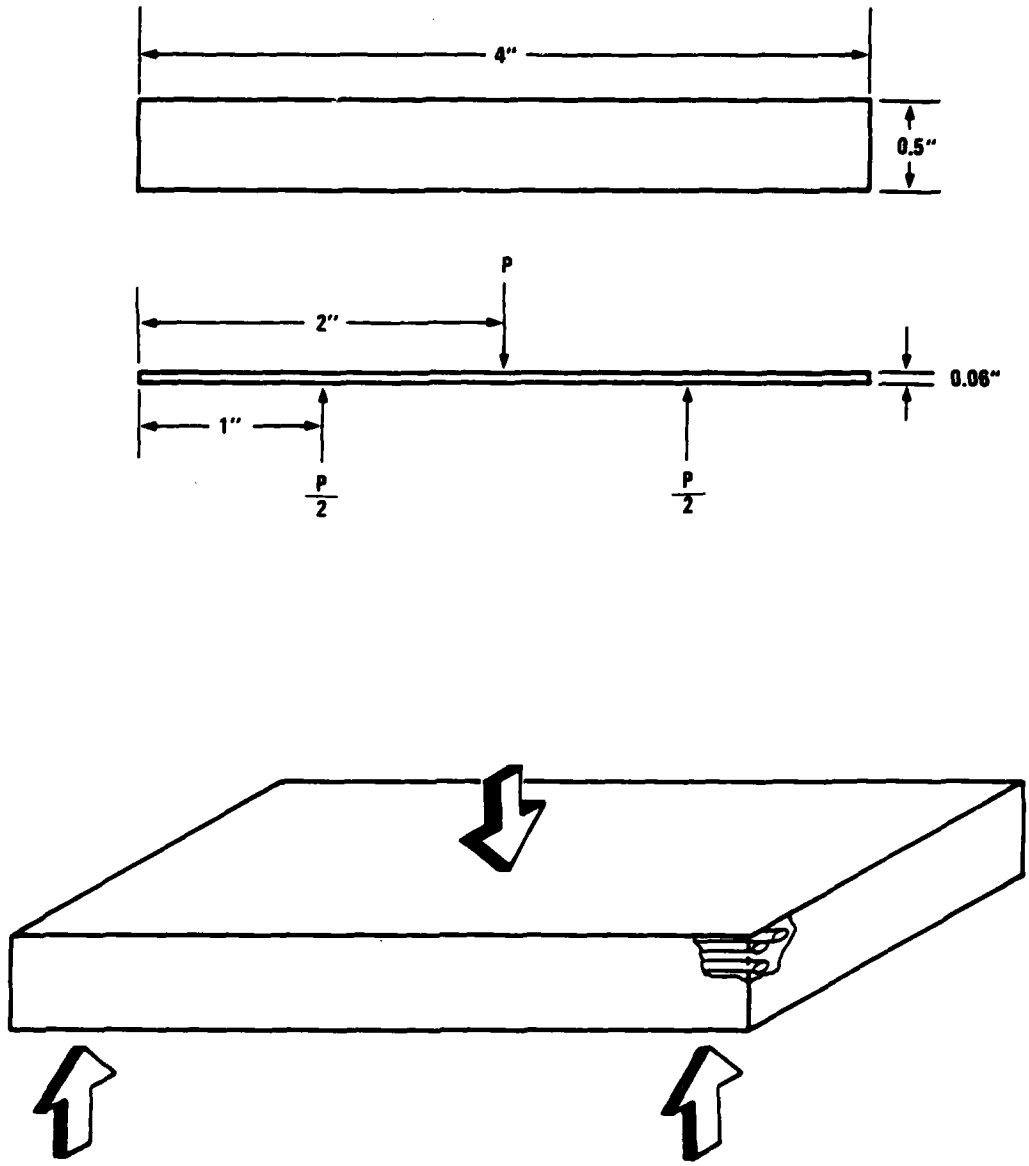


**Figure 11 Three-Point Bend Test Specimens**

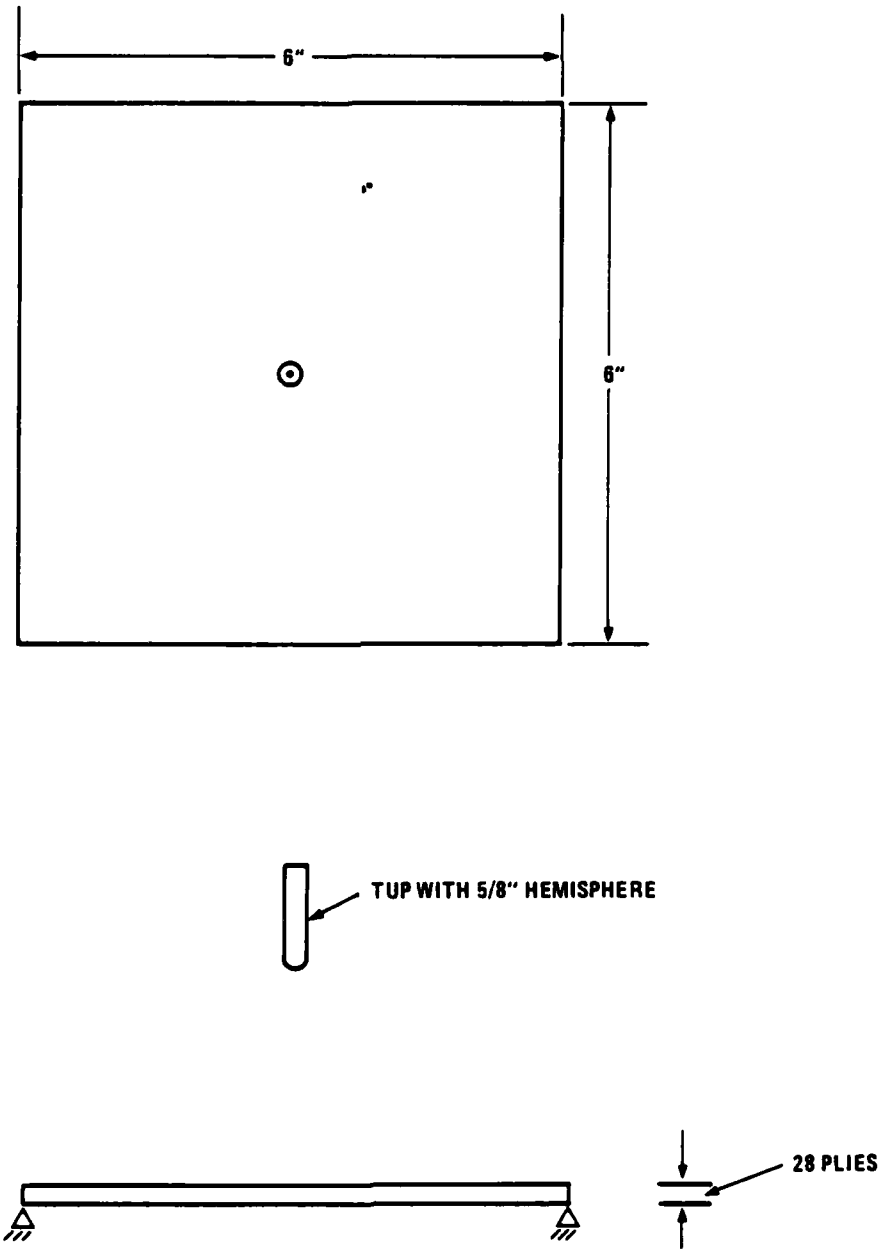


Figure 12 Low Velocity Impact Test Specimen (6.07 Ft Lbs)

## 4.0 FRACTOGRAPHIC RESULTS

The general approach employed in this study has been to examine fundamental specimens which have been subjected to basic loading conditions. As a result, characteristic features have been outlined in a systematic manner. The fractography has concentrated on the features found in the matrix material because this is where the most relevant features are found.

The investigation has shown that the morphology of the various specimens described earlier consists of relatively few characteristic fractographic elements. The presence of any one of these features on a failed specimen does not uniquely define the specimen's failure mode, however. This determination is more subtle because the features are not unique to a single failure mode. Since composite materials are inhomogeneous and their constituents exhibit brittle failure modes, local failure modes (and fractographic features) vary over the fracture surface. For example, while the failure surfaces of the 90° tensile coupons contained features indicative of tensile overload, pockets of elements indicative of shear failure were also found.

Three basic fractographic features have been identified in the matrix material. One involves a shear mechanism while the other two are a result of cleavage mechanisms. These features form the building blocks with which to describe the fracture morphology observed in the different laminae under various loadings. They have been observed in other studies and will now be discussed in order to define them for the purposes of the following discussion.

The feature most commonly observed is a series of epoxy platelets which are due to shear mechanisms. The platelets are raised from the surface and lie on top of one another in a manner analogous to the shingles on a roof. Morris (Ref. 12) referred to them as "hackles" while Sinclair and Chamis (Ref. 6) called them "lacerations". An example of this feature is shown in Fig. 13. This is a 3000X photomicrograph of a series of hackles observed on $G_{12}$ shear specimen 27-3. As the figure shows, this feature is found in the resin material between fibers. The platelets extend from one fiber interface to the other. The relative size and spacing of the platelets varies over the failed surface. Larger, more widely spaced platelets are found in regions where the fibers are relatively further apart. The relative angle of inclination also varies over the failure surface, although in the specimens examined in this study, the

general direction of tilt is consistent over the specimen surface. Regions of tilt reversal were evident on some specimens; however, they were local in nature.

The hackle or laceration was the most prevalent feature encountered on the Mode II, Arcan Shear, and Three Point Bend specimens. It was also present on 90° tension specimens but seemed only secondarily significant there. The platelets are found in both T300/5208 and AS1/3501-6 and are easily detected at 500X magnification.

Two common matrix cleavage features, river patterns and feather patterns, have also been identified. They are analogous to features identified in metallic failure surfaces and have been interpreted in the same way.

River patterns are evident at magnifications of 500X or higher in the resin material between fibers and in resin-rich regions (i.e., resin pockets which form when plies are butted together or at flaws in prepreg tape). The proposed explanation for their formation is that separate cleavage crack segments develop on parallel planes within the matrix regions. As the segments run through the resin, they grow in width and approach each other. Eventually, the crack segments join together fracturing thin ligaments of material and forming steps between the parallel cleavage planes. These steps converge in the direction of local crack propagation. Figures 14 and 15 illustrate typical river patterns found on Mode I type specimens. The pattern in Fig. 14 developed at a resin-rich region within the lamina while the pattern in Fig. 15 illustrates the cleavage of matrix material between fibers.

Another distinct cleavage-fracture feature, the feather pattern or feather mark, was also evident in the failed matrix material. Compared to river patterns, feather marks are more difficult to detect; they have a finer texture and are seen at 3000X or more. They are chevron shaped surface marks which point back in the direction of local crack origin. Figure 16 is a 10000X photomicrograph of the surface of a Mode I specimen in which both river patterns and feather patterns are evident. Complex feather patterns were also found on Mode II specimens. Figure 17 is an example of such a pattern.

It should be noted that the ability to distinguish fracture direction on cleavage surfaces of specific grains may not help in determining the macroscopic fracture direction. Cleavage fracture may take place by very local separation ahead of the moving crack front. Local crack-

Figure 13 Photomicrographs of Hackle Patterns, 3000X

Figure 14 River Pattern in Resin Pocket in Mode I Specimen , 1500X

Figure 15 River Pattern in Resin Material Between Fibers in Mode I Specimen , 1000X

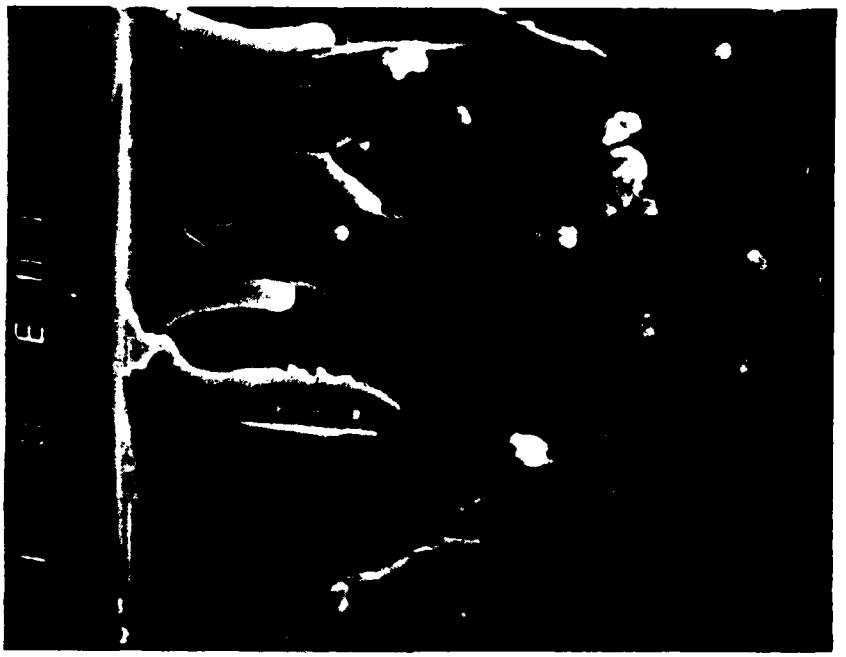

Figure 16 Photomicrograph of Feather Pattern on Mode I Specimen , 10,000X

growth direction is highly dependent on the material. It may be totally unrelated to the macroscopic crack-growth direction, but it still may be used to find the fracture origin.

Figure 18 illustrates typical fiber fracture surfaces. These features were observed in a 0° tensile specimen. As the figure shows, origins and direction of a crack through an individual fiber are detectable by the radial striations imprinted on the fractured fiber surface. Most fiber fractures originate at the fiber's periphery, but some were found to initiate at internal flaws. In many instances, the fracture of two or three fibers may be traced to a common origin at an interfacial point between the fibers. However, an inspection of the whole specimen surface reveals that no global crack propagation direction can be associated with these radial striations as they appear to be randomly oriented.

Two material systems, T300/5208 and AS/3501-6, were used in specimens that were tested under monotonic tension and compression and tension-tension and tension-compression fatigue. The basic fractographic features described above were common to both material systems. Furthermore, the combinations of fractographic features for the same specimens subjected to the same loading were the same for both materials. In the review of the examination of the specimens that now follows, comments referring to one particular material may therefore be taken to apply to the others.

## 4.1 Shear Specimens

The shear specimens that were examined in this study had been used to determine, among other quantities, the shear moduli $G_{12}$, $G_{23}$ and $G_{31}$. There was no difference between the specimens used to determine $G_{12}$ and $G_{31}$. This is not surprising because the fiber orientation is the same in both cases (Figure 8).

Figure 19 consists of macroscopic and microscopic views of the fracture surface of a typical $G_{12}$ shear specimen. The test conditions, failure stress and the primary fractography characteristics are itemized on the figure data sheet. A macroscopic view of a typical failed specimen is shown in Fig. 19a. A 5X photograph of the specimen which has been removed from its aluminum loading rings demonstrates that the failure surfaces were planar on a macroscopic scale. Specimen damage was confined to the

Figure 17 Photomicrograph of Feather Pattern on Mode II Specimen, 5000X

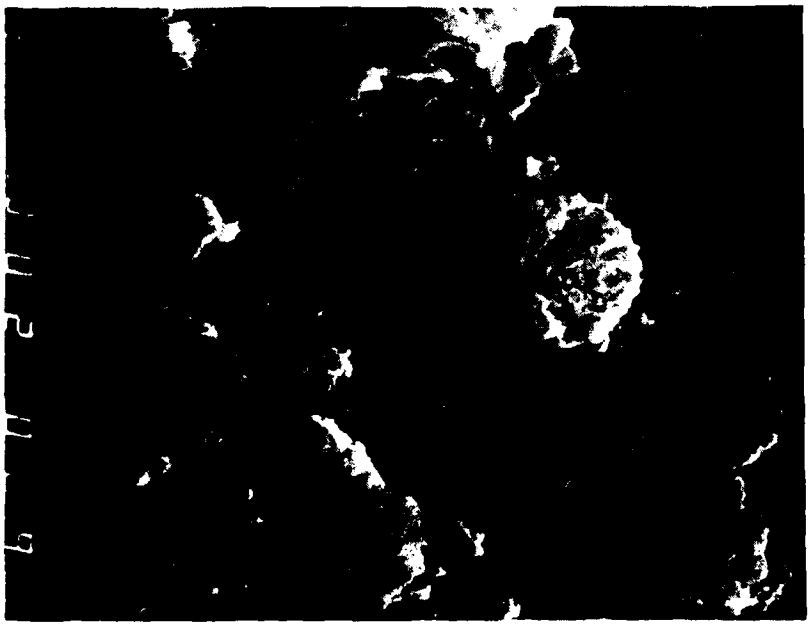

Figure 18 Typical Fiber Fracture Surfaces, 3000X

Figure 19 ARCAN SHEAR ($G_{12}$)

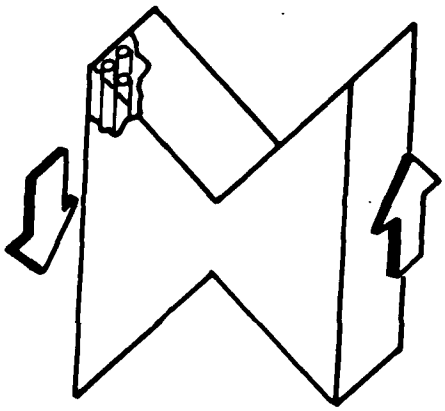

| | |
|---|---|
| Specimen: | 29-3 |
| Stress State | $\tau_{12}$ |
| Ultimate Stress | 10.60 ksi |
| Average (of 5) | |
| Ultimate Stress | 9.44 ksi |
| Material: | T300/5208 |
| Test Rate | 0.02 in/min |
| Environment | Ambient |
| Initial Defects | Notched |
| Failure Sequence | Catastrophic across notched area |

Primary Failure Surface Characteristics

| Figure | Characteristic |
|---|---|
| a | Planar Fracture Surface (macroscopic) |
| b,c | Hackles of Varied Inclination |
| c,d | Feathered Scallops |

Figure 19a Macroscopic Views of Typical $G_{12}$ Shear Specimen, 5X and 14X

(b) 5000X

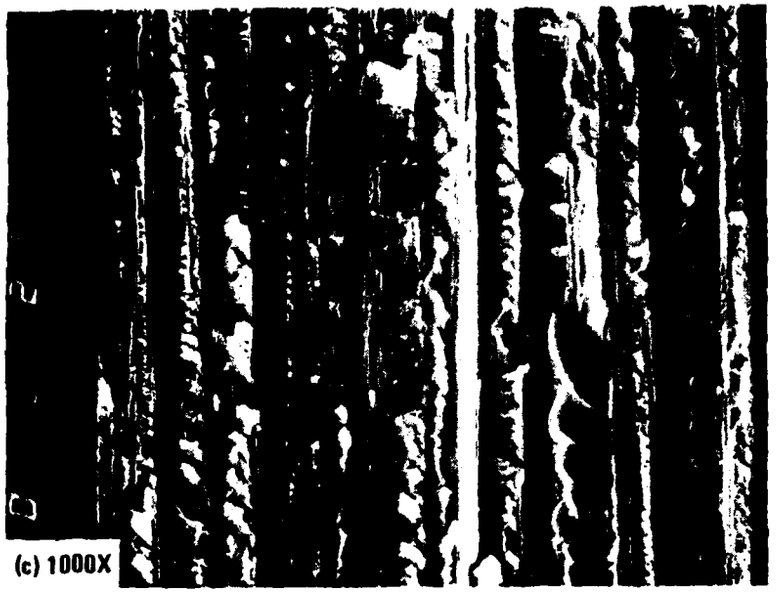

(c) 1000X

(d) 5000X

Figures 19b, c, and d Photomicrographs of G12 Shear Specimen Surface

failure site. Fig. 19a also has a 14X macroscopic photograph of the two failed surfaces. Again the surfaces appear planar, but local regions of fiber pullout are evident, giving the surfaces a rough or "rutted" appearance.

Figure 19b, c, d are SEM photomicrographs of the fracture surface. Relatively few fiber breaks were observed over the specimen. The key surface features were hackle patterns in the epoxy resin between the fibers. These raised patterns showed consistent orientation over each fracture surface. Although the angle of inclination varied in regions, the general tilt direction was constant.

Figure 20 shows a typical region of a $G_{31}$ shear specimen surface. It contains three photographs (b, c, and d) of the same area taken at 200X, 500X and 1000X. The raised epoxy platelets are particularly evident at higher magnifications. Regions of the matrix material also displayed curved surfaces where it appeared the material had been "scooped" away. Feather patterns are evident on the surfaces of these scooped or "scalloped" regions at higher magnifications. Note the similarity between the $G_{12}$ and the $G_{31}$ surfaces shown in Figs. 19 and 20, respectively.

Surface features on the mating surface were composed of the same elements. Hackles or lacerations were predominant. Again the hackle tilt direction was consistent throughout the surface, but now the hackles were inclined in the opposite direction. This reversal is demonstrated in Fig. 20e. It is a 500X photomicrograph of the area believed to be the mating surface of the area shown in Fig. 20b, c, d. Similar reversal was reported by Morris in his study of notched tensile specimens (Ref. 12).

Unlike the $G_{12}$ and $G_{31}$ specimens discussed above, the $G_{23}$ shear specimens had curved failure surfaces. A possible explanation is that cracking initiated at the specimen notch and changed direction while propagating through the specimen. Since fibers are perpendicular to the plane in which load is applied, the crack must travel over and around fibers (i.e., in a path of minimum resistance). This was not the case in the $G_{12}$ and $G_{31}$ specimens because, in propagating through those specimens, the crack front progressed along the fibers. Once initiated, crack front propagation was restricted to one plane (macroscopically) since deviation from that plane would require extensive fiber breakage. Macroscopic photographs of a typical $G_{23}$ specimen are shown in Fig. 21. Figure 21a (a 4X view of the specimen face) shows the curved fracture path. Figure 21b shows mating failure surfaces.

Figure 20 ARCAN SHEAR ($G_{31}$)

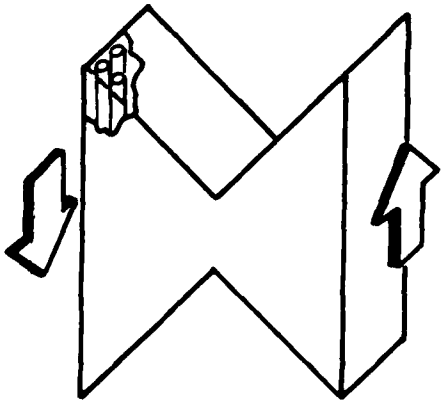

| | |
|---|---|
| Specimen: | 27-2 |
| Stress State | $\tau_{31}$ |
| Ultimate Stress | 7.72 ksi |
| Average (of 4) | |
| Ultimate Stress | 7.43 ksi |
| Material: | T300/5208 |
| Test Rate | 0.02 in./min. |
| Environment | Ambient |
| Initial Defects | Notched |
| Failure Sequence | Catastrophic across notched area |

Primary Failure Surface Characteristics

| Figure | Characteristic |
|---|---|
| a | Planar Fracture Surface (macroscopic) |
| b,c,d,e | Hackle Pattern of Varied Inclinations |

14x

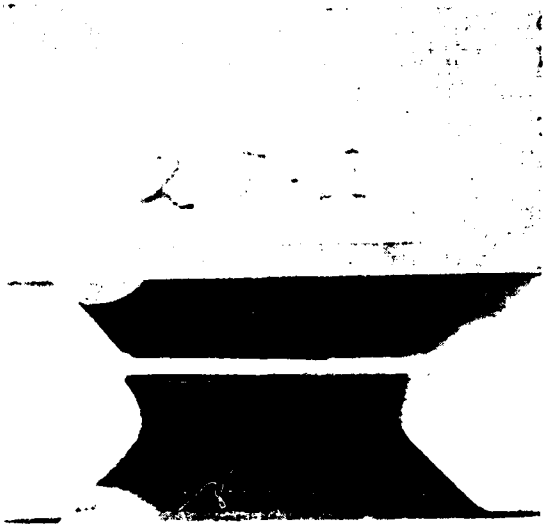

3x

Figure 20a Macroscopic Views of $G_{31}$ Shear Specimen

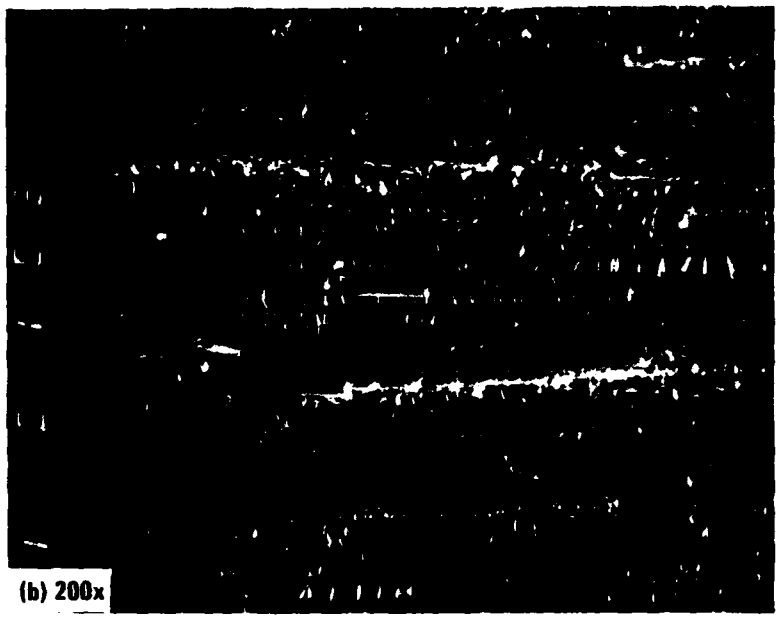

(b) 200x

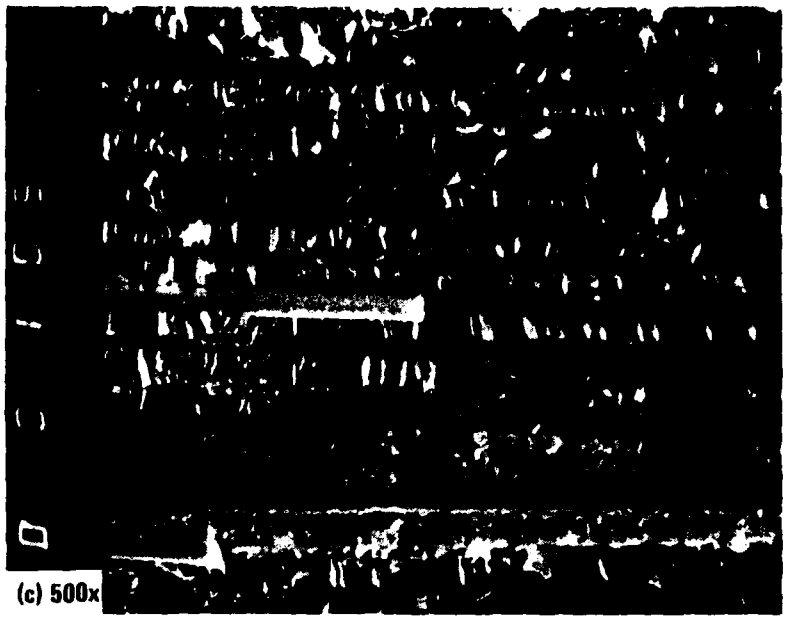

(c) 500x

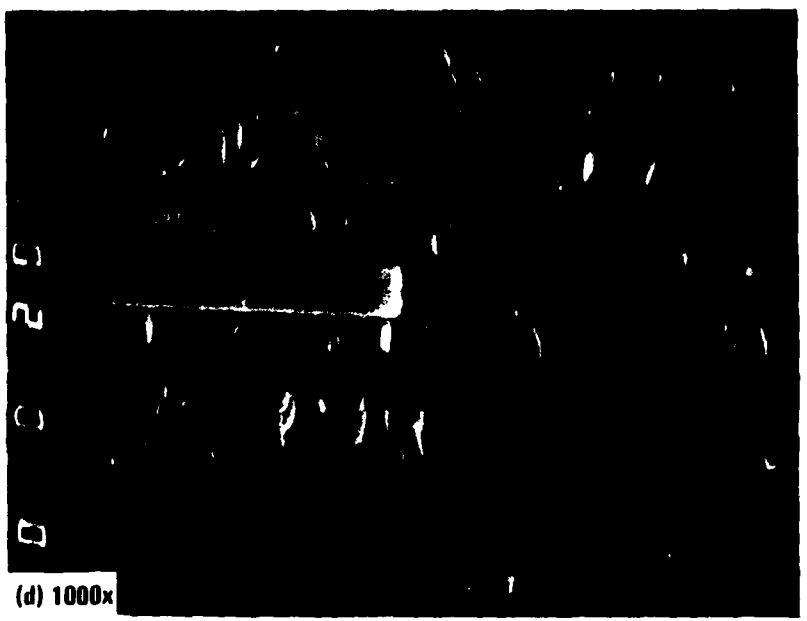

(d) 1000x

Figure 20b, c, and d Photomicrographs of the Same Region of a $G_{31}$ Fracture Surface

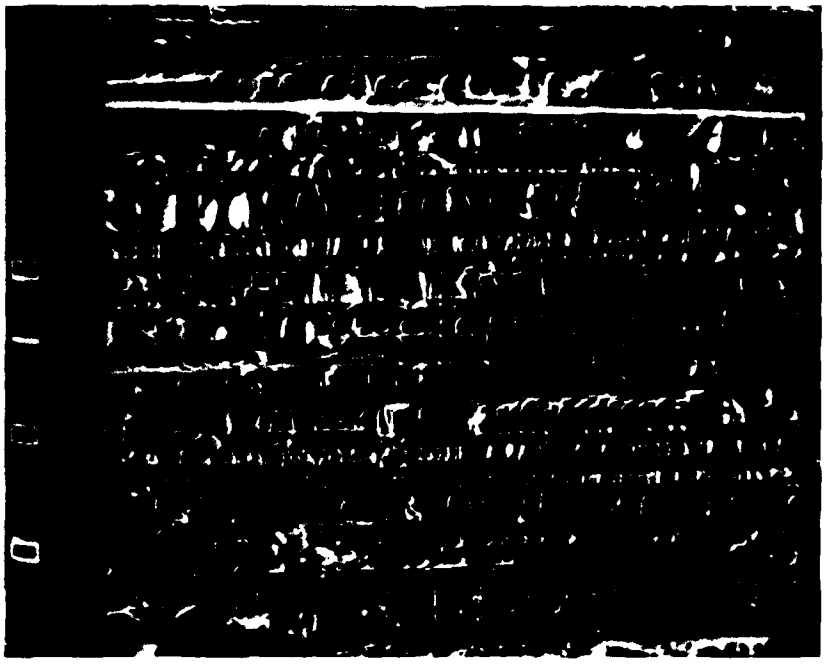

Figure 20e Photomicrograph of Shear Specimen Surface, 500x

Figure 21 ARCAN SHEAR ($G_{23}$)

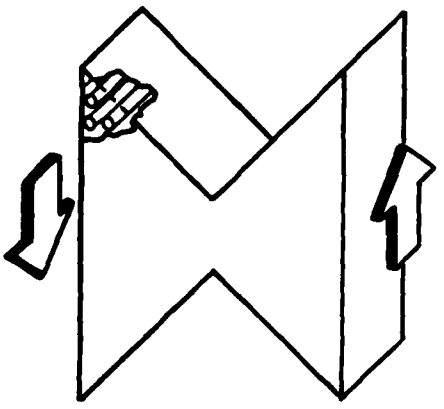

| | |
|---|---|
| Specimen: | 25-2 |
| Stress State | $\tau_{23}$ |
| Ultimate Stress | 4.72 ksi |
| Average (of 3) | |
| Ultimate Stress | 5.08 ksi |
| Material: | T300/5208 |
| Test Rate | 0.02 in./min. |
| Environment | Ambient |
| Initial Defects | Notched |
| Failure Sequence | Catastrophic across notched area |

Primary Failure Surface Characteristics

| Figure | Characteristic |
|---|---|
| a | Failure Surface (macroscopic) |
| b | Curved Fracture Surface (macroscopic) |
| c | Shear Surface |
| d | Cleavage Features, River Patterns, Fiber Pullout, Resin Strips |

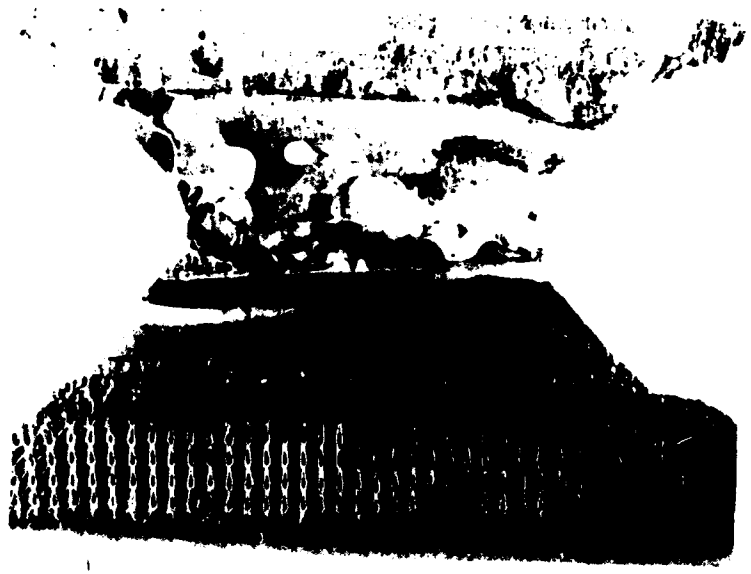

Figure 21a Macroscopic View of $G_{23}$ Shear Specimen, 4x

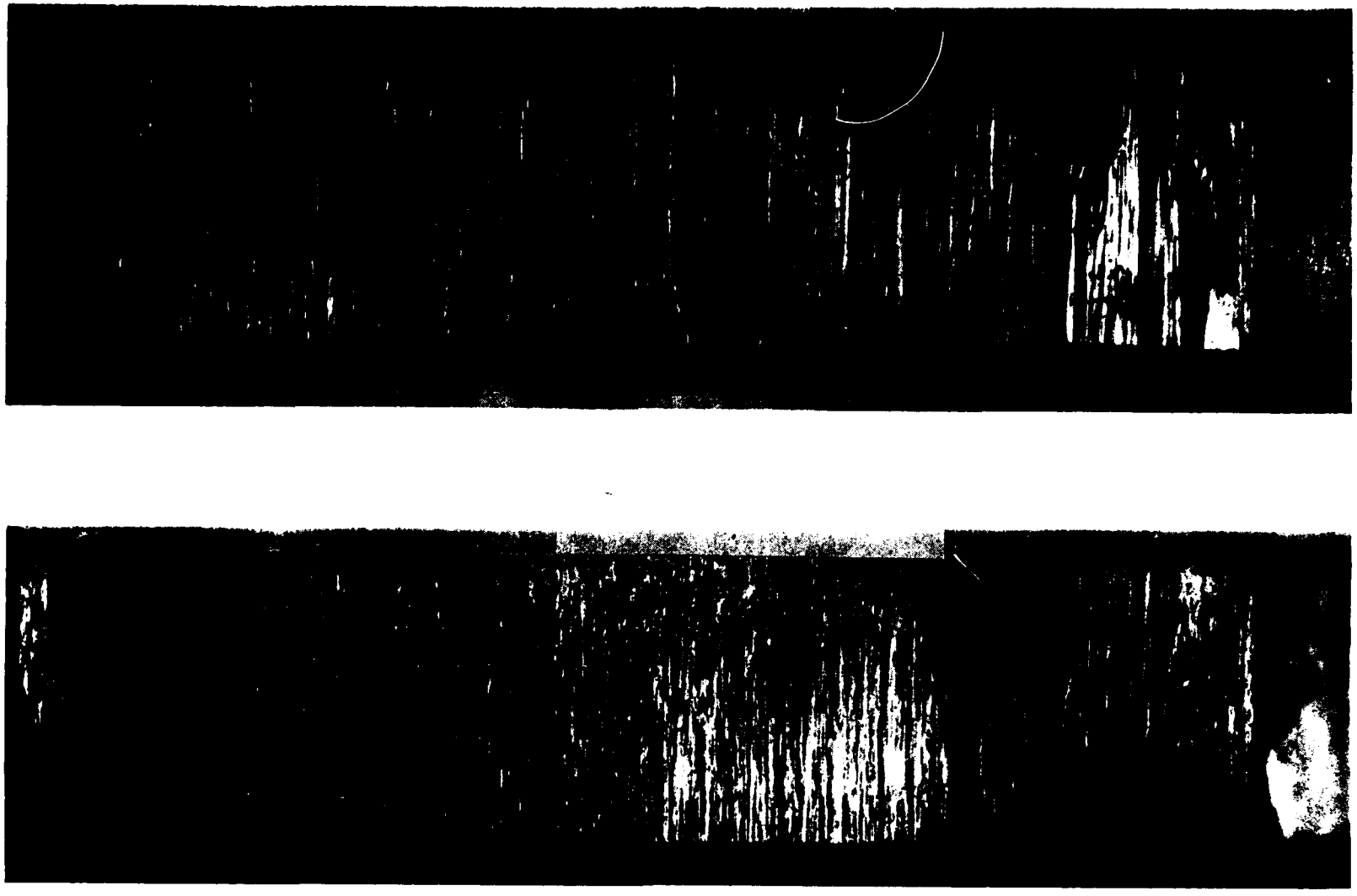

Figure 21b Macroscopic View of $G_{23}$ Shear Specimen Surfaces, 14x

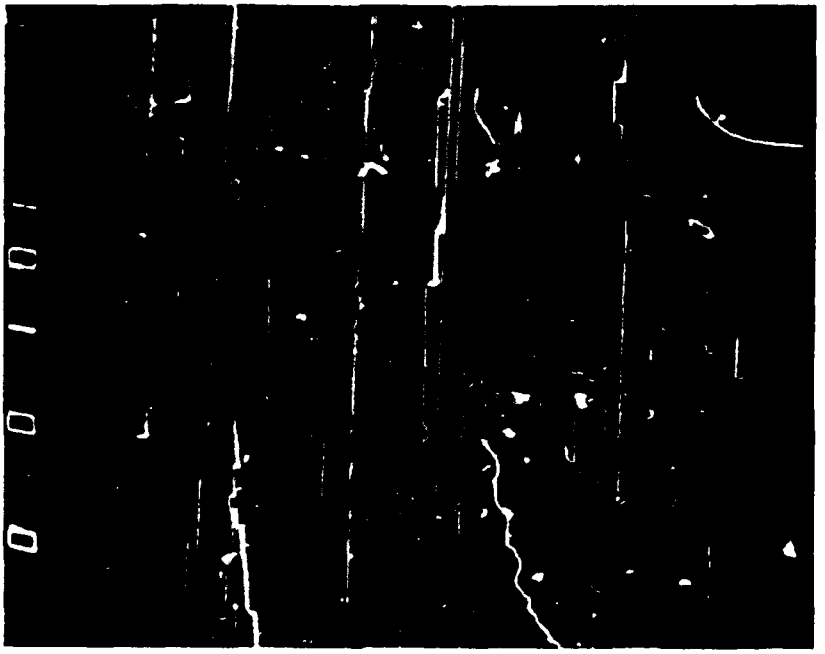

Figure 21c Photomicrograph of $G_{23}$ Shear Specimen Surface, 100x

Figure 21d Photomicrograph of $G_{23}$ Shear Specimen Surface, 430x

The $G_{23}$ specimens also differed from the $G_{12}$ and $G_{31}$ specimens on the microscopic level. Investigation showed that none of the characteristic hackle features developed on the specimens. Instead, matrix artifacts consisted of cleavage features (i.e., river patterns). Figure 21c is a 100X photomicrograph of a typical specimen section. Several cavities which once contained fibers are evident on the specimen surface. The resin material which surrounds these voids appears to be relatively undisturbed. (This observation is verified in Fig. 21d). The bright curved feature which appears in the upper right corner of the photograph is a sliver of matrix material which has been partially stripped away from the adjacent fiber. These stringers were found throughout the failed surface. Figure 21d is a micrograph of that same stringer. The figure also demonstrates the development of river patterns in the matrix material between fibers. These cleavage features were also evident throughout the specimen. The river patterns and the position of the matrix stringer indicate that, at least locally, the crack front progressed from left to right.

## 4.2 Mode I Fracture Specimens

The surfaces of the Mode I specimens were also largely planar on a macroscopic scale. Figure 22a shows mating section of a typical specimen at 2X. The surfaces have a rather smooth texture although broken fibers were evident at higher magnifications. The patterns of concentric arcs which appear on the specimen surfaces in these photographs taken with an indirect light source were not evident when the specimen was examined in the SEM.

Cleavage features dominated the fracture surface detail. Feather and river patterns were the prime features of note. They were seen in the matrix material between fibers as shown in Figs. 15 and 22b and in pockets of resin-rich regions as shown in Fig. 22c. As mentioned in the earlier discussion of river patterns, the patterns converge or flow in the direction of local crack propagation. As a rule, the patterns were indicative of the general direction of crack propagation on these specimens. However, Fig. 22d illustrates an exception to that rule. Although the river patterns on the left side of the figure indicate that local crack propagation is from right to left, the global direction of propagation is known to be from the bottom of the picture to the top.

Figure 22 Mode I Fracture

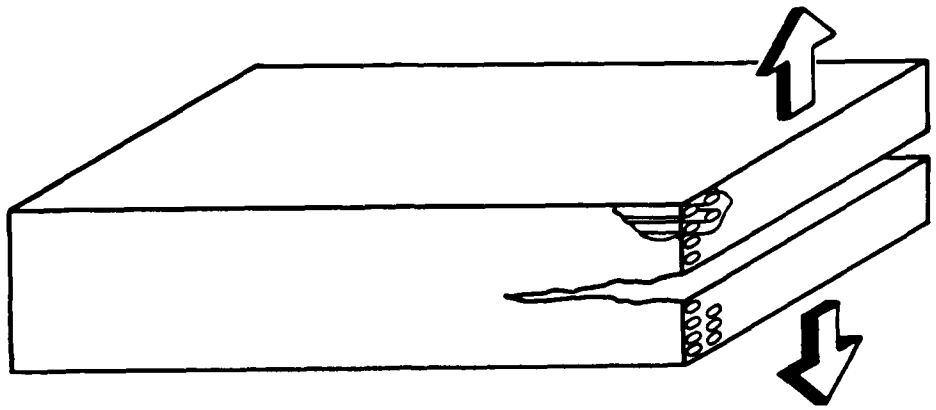

| | |
|---|---|
| Specimen: | 097-1-208 |
| Stress State | $\sigma_{33}$ |
| Critical Strain Energy Release Rate ($G_{IC}$) | * |
| Average (of 3)($G_{IC}$) | 0.335 (in-lbs)/in$^2$ |
| Material: | T300/5208 |
| Test Rate | 0.02 - 0.05 in./min. |
| Environment | Ambient |
| Initial Defects | Starter Crack |
| Failure Sequence | Starter Crack propagates in a stepwise fashion each time $G_{Ic}$ is obtained. |

**Primary Failure Surface Characteristics**

| Figure | Characteristic |
|---|---|
| a | Fracture Surface (macroscopic) |
| b,c | River and Feather Patterns |
| d | River Patterns |

*Data not available for this specimen.

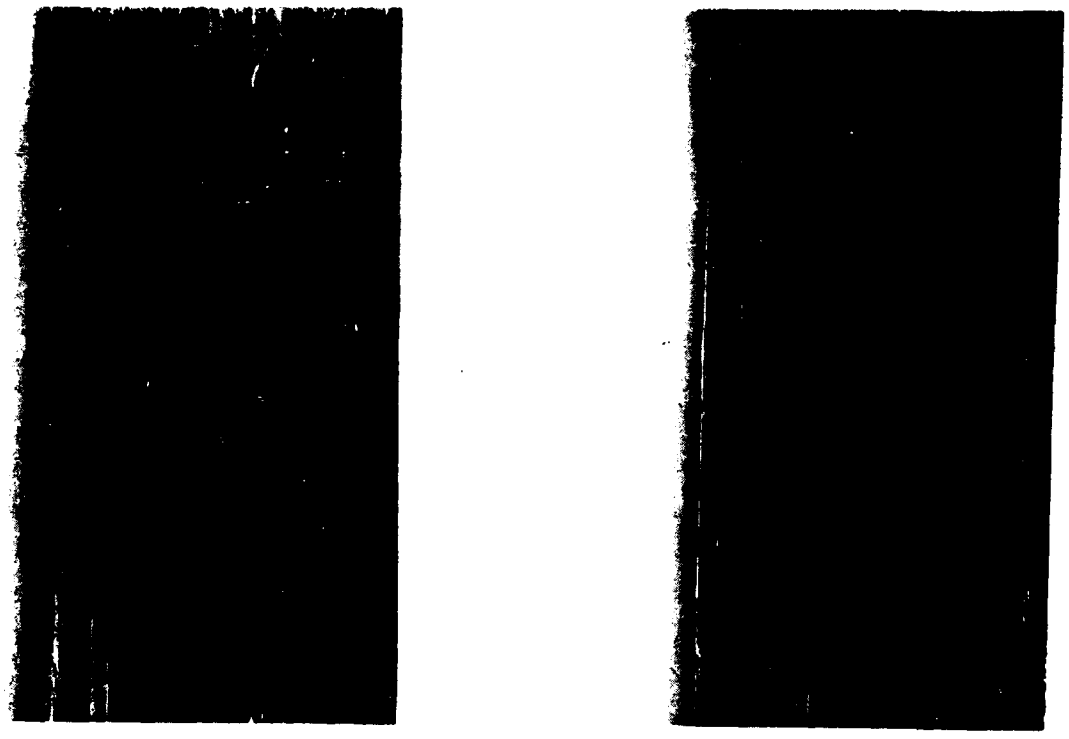

Figure 22a Macroscopic View of Mode I Fracture Specimen Surface , 2X

Figure 22b River Patterns on Mode I Fracture Surface,500x

Figure 22c River Patterns on Mode I Fracture Surface,500x

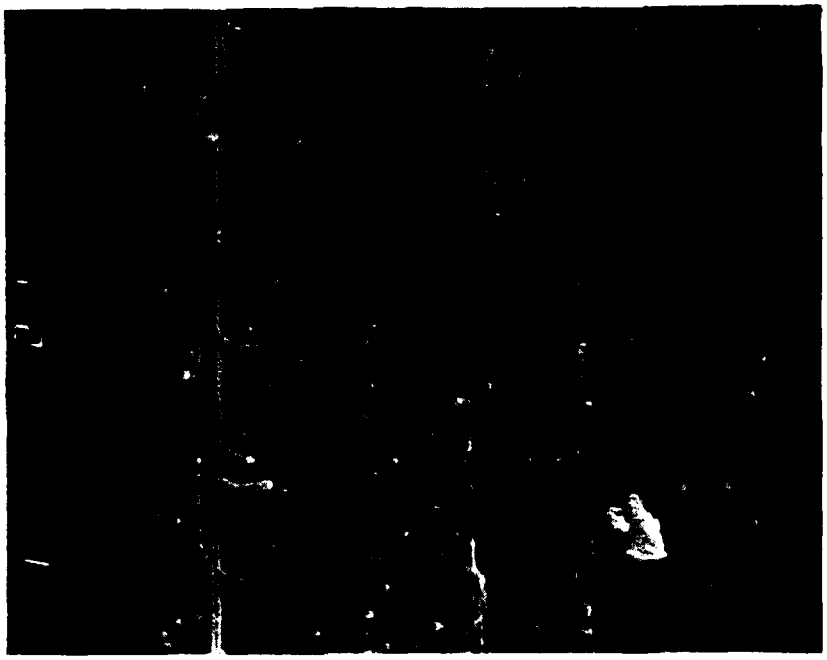

Figure 22d Photomicrographs of River Patterns on Mode I Specimen , 2000X

## 4.3 Mode II Fracture Specimens

The macroscopic differences between Mode I and Mode II failure surfaces are displayed in Fig. 23a. This is a photograph of a Mode II coupon which was mechanically tested growing a Mode II crack then pulled apart causing a Mode I surface. On a macroscopic level, the differences are evident. Microscopically, the Mode II specimen surface features were identical to those found on the $G_{12}$ and $G_{31}$ butterfly shear specimens. Hackles were again the prime fractographic components. The general tilt direction was consistent over the surface and was reversed on the mating surface. Even at 200X (Fig. 23b) the similarity of the two surface types is evident. Figure 23c is the 1000x photograph of the region in the left center in Fig. 23b. The figure illustrates several well defined hackle patterns and shows a unique scalloped region., At 5000X (Fig. 23d) feather patterns are evident on the faces of the scalloped matrix material. The feather marks describe a complex swirling pattern in the resin which wraps around the fiber. The figure indicates that the fiber was not fractured and that the local matrix cleavage crack was forced to flow around the fiber.

Another scalloped region is shown in the lower right portion of Fig. 23e along with several other well developed hackle patterns (lower left portion). The feather patterns developed on these scalloped features were illustrated in Fig. 17.

## 4.4 Three Point Bend Specimens

The three point bend specimens reviewed in this study are used by GD/FWD to determine the 0° flexural modulus. This property is used as one of the criteria for determining the acceptability of incoming graphite/epoxy prepreg material. Figure 24a illustrates the edge view of several failed specimens. Tensile fiber failure occurred at the point of maximum tensile stress (outside surface at midpoint along the span). As the initial fibers broke, load was transferred to the adjacent fibers which were subsequently overloaded. This resulted in damage development which propagated through the thickness. The figure also illustrates that delamination developed at these fiber breaks and propagated away from the fiber breaks toward the specimen ends. Figure 24b, c shows photomicrographs of specimen 23B1-3.

A typical section of the broken fiber surface is shown in Fig. 25b. The fibers form an irregular, jagged line

Figure 23 Mode II Fracture

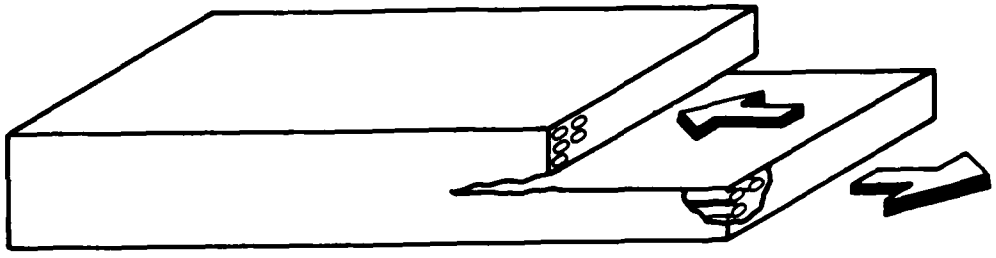

| | |
|---|---|
| Specimen: | 098-1-2 |
| Stress State | $\tau_{13}$, $\sigma_{11}$ |
| Critical Strain Energy Release Rate ($G_{IC}$) | * |
| Average (of 3)($G_{IC}$) | 1.1 (in-lbs)/in$^2$ |
| Material: | T300/5208 |
| Test Rate | 0.01 in/min |
| Environment | Ambient |
| Initial Defects | Starter Crack |
| Failure Sequence | Starter crack propagates in a step-wise fashion each time $G_{IIc}$ is reached. |

Primary Failure Surface Characteristics

| Figure | Characteristic |
|---|---|
| a | Mode I (left) and Mode II (right) Fracture Surfaces on a Mode II Coupon (macroscopic) |
| b | Fracture Surface |
| c,e | Hackle Patterns |
| d | Feather Patterns |

*Data not available for this specimen

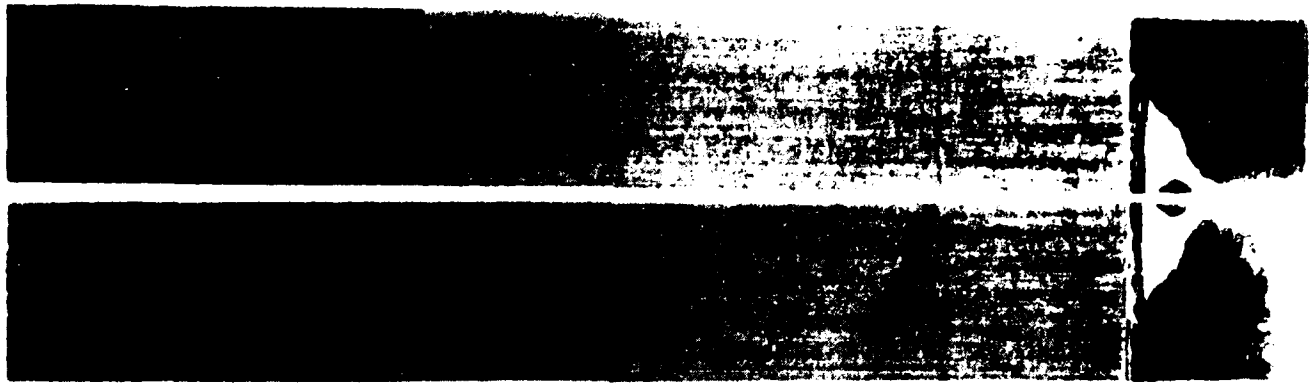


Figure 23a Macroscopic View of Mode II Fracture Surface, 1x

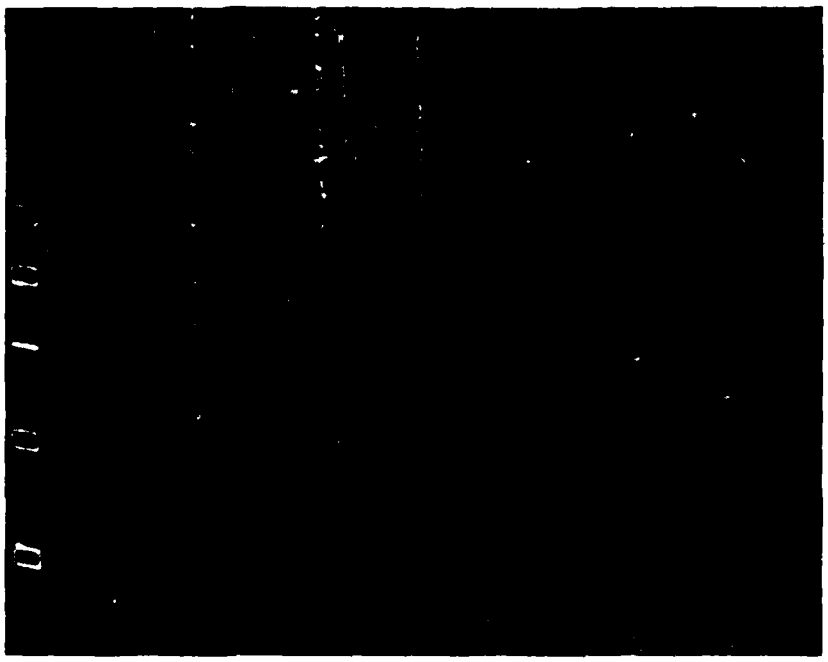

Figure 23b Photomicrograph of Mode II Specimen Surface , 200X

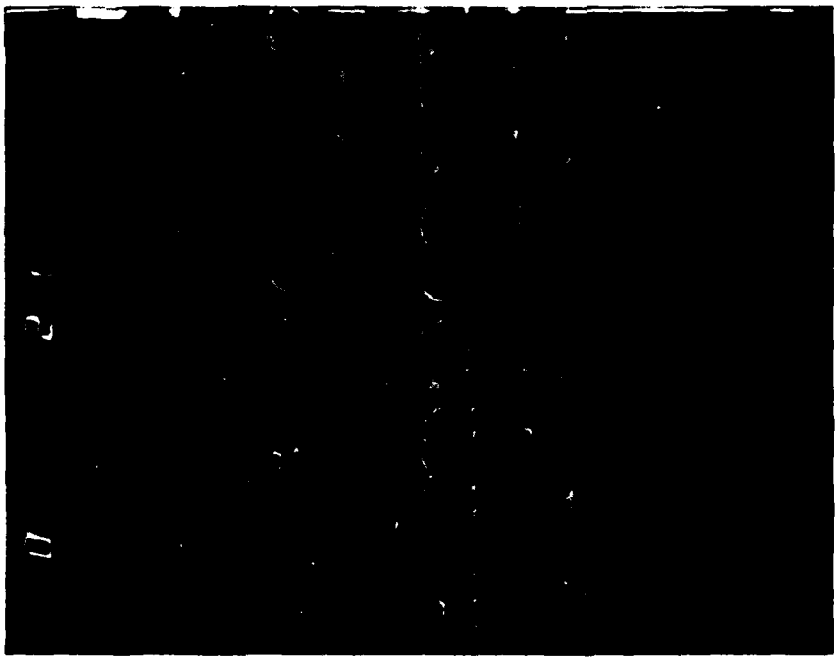

Figure 23c Photomicrograph of Mode II Specimen Surface,1000x

Figure 23d Feather Patterns on Mode II Specimen, 5000X

Figure 23e Photomicrograph of Mode II Specimen Surface, 1000x

Figure 24 $0^{\circ}$ Flexture (1)

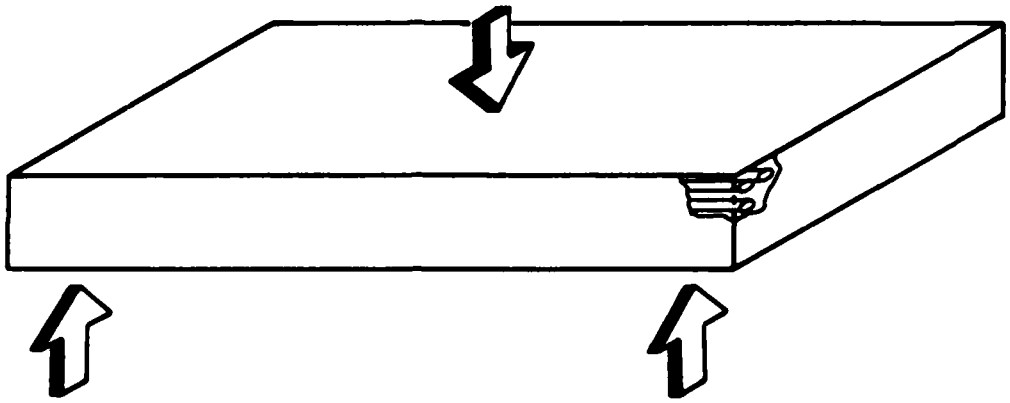

| | |
|---|---|
| Specimen: | 23B1-3 (roll 23B) |
| Stress State | $\sigma_{11}$, $\tau_{13}$ complex |
| Ultimate Stress | * |
| Average (of 2) | |
| Ultimate Stress | 265.5 ksi |
| Material: | AS1/3502 |
| Test Rate | 0.05 in./min. |
| Environment | Ambient |
| Initial Defects | None |
| Failure Sequence | Fiber Failure of bottom ply (Maximum Tensile Stress) followed by multiple delamination due to shearing stresses |

Primary Failure Surface Characteristics

| Figure | Characteristic |
|---|---|
| a | Fracture Mode (macroscopic) |
| b | Stairstep Pattern of Broken Fibers Leads to Spire Peaks |
| c | Hackle Patterns found on Delaminated Surface |

*Data unavailable.

23B1-2

23B1-3

Figure 24a Macroscopic View of Three Point Bend Specimens, 3X

23B1-2

23B1-3

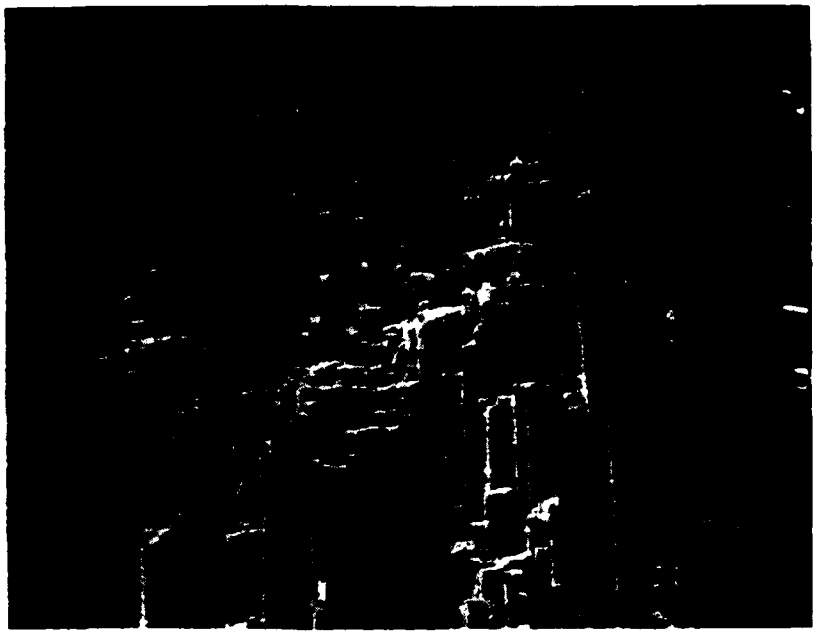

(b) 200X

(c) 1000X

Figures 24b and c Photomicrographs of Three-Point-Bend Specimen Surfaces

which extends across the specimen width. Figure 25c is a 100X fractograph of a typical broken fiber spire (found in the right side of Fig.25b). A stairstep pattern of broken fibers leads to the peaks of the spires. Hackle patterns identical to those found on the Mode II specimens and the shear specimens are also evident in the figure. These raised epoxy platelets again appeared to be the major fractographic feature. Figure 25d provides a closer view of a representative pattern found a short distance from the fiber break line. The hackles had a consistent tilt direction in these regions of the specimen. However, as Fig. 25e illustrates, the direction of tilt was reversed on the opposite side of the line of broken fibers (i.e., the hackles point back toward the fracture site). As in the other cases, hackle pattern reversal was also seen on mating surfaces in the three point bend specimens. Comparing the microscopic surfaces observed in Figures 24 and 25, no substantial differences are noted. This is despite substantial differences in the ultimate strengths of the various batches of material these specimens came from.

## 4.5 Tension Specimens

### 4.5.1 90° Laminae

Like the $G_{12}$ and $G_{31}$ shear specimens, the failure surfaces on the 90° tension specimens were also macroscopically planar. A 2X enlargement of a typical specimen is shown in Fig. 26a. Failure occurred on a plane perpendicular to the applied load (parallel to the fibers) and damage appeared to be restricted to the failure site. A typical section of a failed surface is shown in Fig. 26b. Again, like the $G_{12}$ and $G_{31}$ shear specimens, the surface has a rough or rutted texture indicating that the failure plane is established by the packing array of the fiber tows.

Mixed failure modes were evident on the specimen surfaces. This was reflected in the fractographic features found in some locations while cleavage features were evident at other locations. Figure 26c is a 500X photomicrograph of a typical specimen section. Hackle patterns are evident at the bottom of the figure while the resin material in the rest of the photograph has a mottled appearance. This latter feature appears to be representative of a pure 90° tensile failure. The flat matrix features seem indicative of cleavage type failure, but unlike the Mode I features, flow lines indicating crack propagation direction were not immediately discernable.

Figure 25 $0^{o}$ Flexture (2)

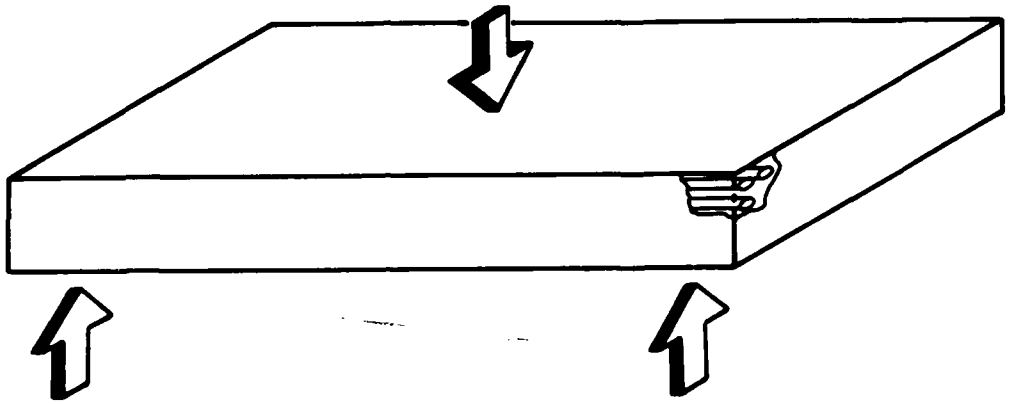

| | |
|---|---|
| Specimen: | 19B3-C (roll 19B) |
| Stress State | $\sigma_{11}$, $\tau_{13}$ (complex) |
| Ultimate Stress | * |
| Average (of 9) | |
| Ultimate Stress | 168.2 ksi |
| Material: | AS1/3502 |
| Test Rate | 0.05 in/min |
| Environment | Ambient |
| Initial Defects | None |
| Failure Sequence | Fiber failure of bottom ply (Maximum Tensile Stress) followed by multiple ply delamination due to shearing stresses. |

Primary Failure Surface Characteristics

| Figure | Characteristic |
|---|---|
| a | Fracture Mode (macroscopic) |
| b,c | Fiber Spines |
| d,e | Hackles on Delaminated Surface |

*Data unavailable.

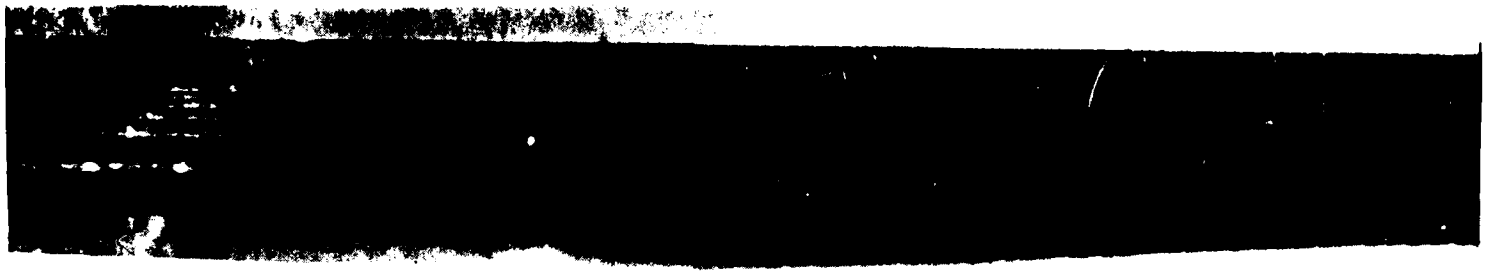

Figure 25a Macroscopic View of Three-Point Bend Specimen, 6x

Figure 25b Typical Broken Fiber Surface on Three Point Bend Specimen, 27X

Figures 25c Fractograph of Broken Fibers, 100x

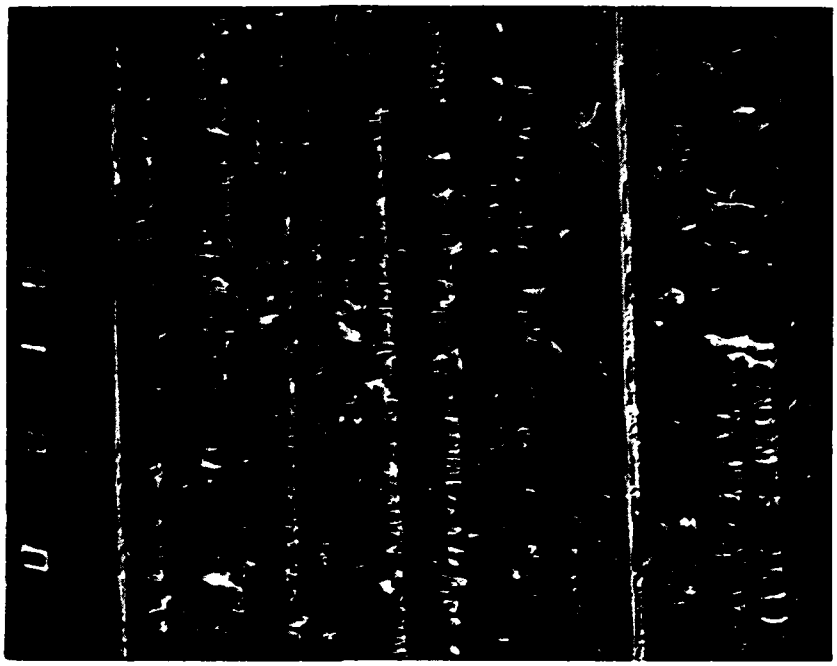

Figure 25d Hackle Pattern on Three Point Bend Specimen, 500x

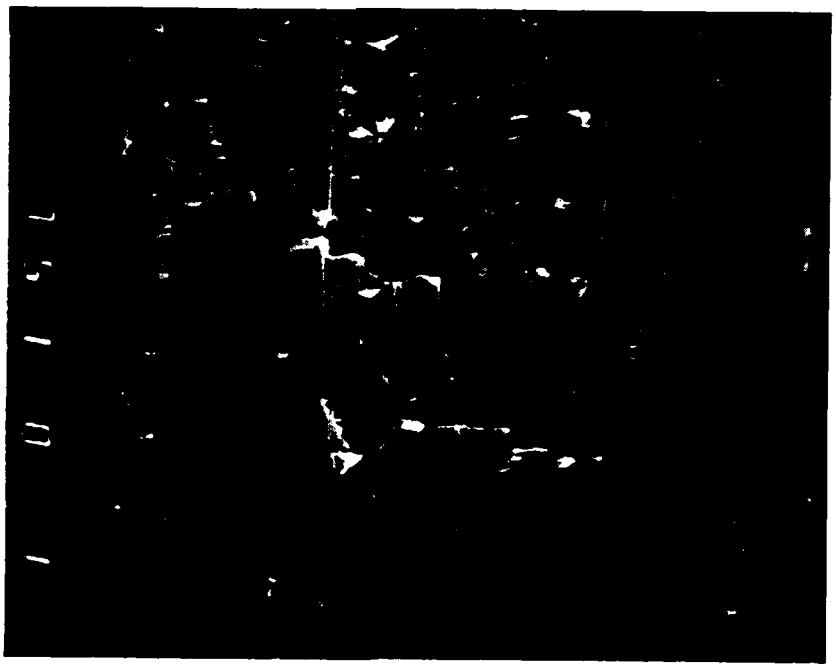

Figure 25e Tilt Reversal at Fiber Breaks in Three Point Bend Specimen, 750x

Figure 26 $90^{\circ}$ Tension

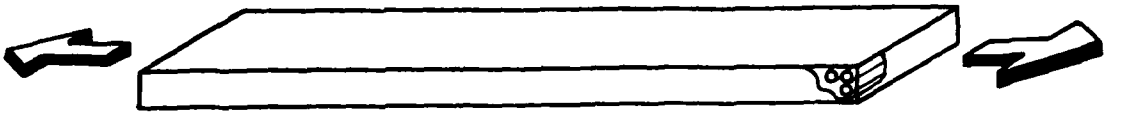

| | |
|---|---|
| Specimen: | T90 - T6 |
| Stress State | $\sigma_{22}$ (Tension) |
| Ultimate Stress | 8.15 ksi |
| Average (of 9) | |
| Ultimate Stress | 7.28 ksi |
| Material: | T300/5208 |
| Test Rate | 0.05 in/min |
| Environment | |
| Initial Defects | None |
| Failure Sequence | Catastrophic |

Primary Failure Surface Characteristics

| Figure | Characteristic |
|---|---|
| a | $90^{\circ}$ specimen failure (macroscopic) |
| b | Failure Surface (macroscopic) |
| c | Mixed mode failure patterns:<br>Hackle patterns (bottom)<br>Cleavage |

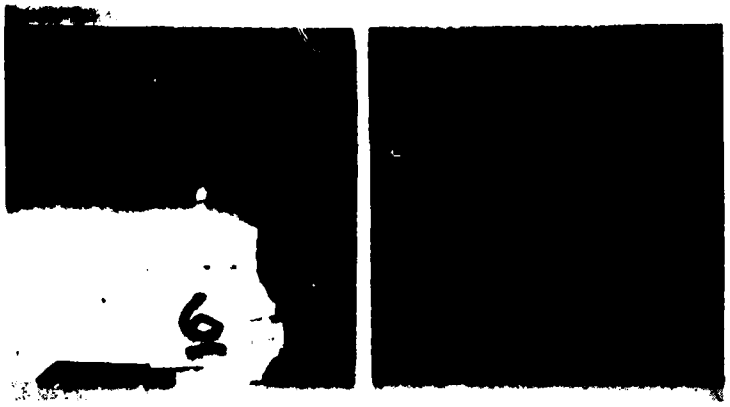

Figure 26a Macroscopic View of 90° Tensile Specimen , 2X

Figure 26b Macroscopic View of 90° Tensile Specimen Surface , 9X

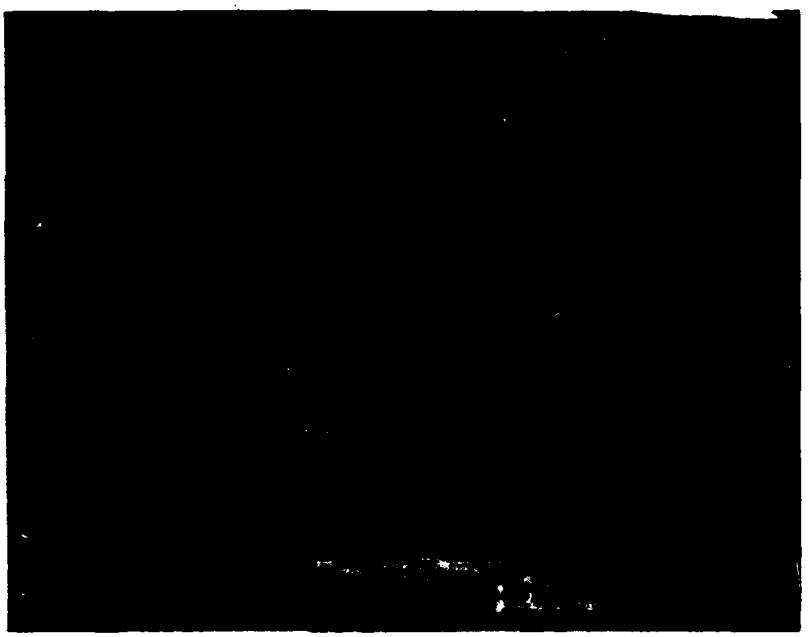

**Figure 26c Photomicrograph of 90$^0$ Tensile Specimen , 500X**

### 4.5.2 0° Laminae

A macroscopic view of the overall fracture topography of the 0° tensile specimens is typified by Fig. 27a. As can be seen, the contour of the fractured surface is very irregular (just as in the three point bend specimens). The catastrophic release of energy at failure resulted in extensive longitudinal matrix cracking. Longitudinal cracks often extended along the entire specimen length.

On the microscopic level, the general fracture topography takes the form of two repeated features. The first consists of blunted spires arranged in a random array while the second is made up of rows of stairsteps containing diagonally fractured fibers which appear to have failed in shear. Although both features were seen to some degree on all specimens, the former is by far the more predominant feature. Examples of both are seen in Figure 27b.

The matrix fracture in the plane of the crack contains smooth cleavage facets while the fibers have a rough irregular cross-section. As mentioned earlier, the origin and direction of crack propagation through individual fibers is detectable by the radial striations imprinted on the fractured fiber surfaces. However, it does not seem possible to assign a global crack propagation direction from these features because their relative orientation appears almost random. Figure 18 shows a typical broken fiber section.

Finally, the surfaces of the long matrix cracks which extended along the specimen length bore the distinctive hackle pattern marking observed before demonstrating the possible presence of interfacial shear.

### 4.5.3 $[\pm 45]_{4S}$ Laminae

The failure of ±45° laminae under tension (Fig. 28a,b) is initiated by transverse cracking of the middle two +45° plies at various locations along the length of the coupon. This is followed by transverse cracking in the -45° plies on either side of the two central +45° plies. Figure 29 is a schematic depicting the locations of the transverse cracks as they spread to the outermost +45° and -45° plies. It is very noticeable that the cracks intersect the specimen edge at approximately the same axial location for the same orientation of lamina. When viewed in plan form (Fig. 29) this gives the appearance of a band of transverse cracks. Furthermore, it was very often the case that the two bands

Figure 27 $0^{\circ}$ Tension

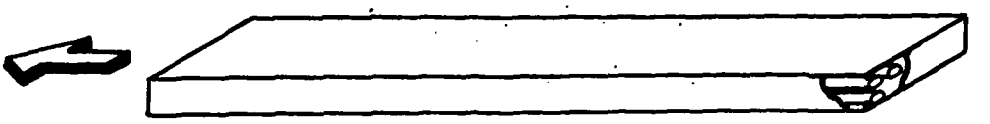

| | |
|---|---|
| Specimen: | T0 - A6 |
| Stress State | $\sigma_{11}$ (Tension) |
| Ultimate Stress | 262 ksi |
| Average (of 8) | |
| Ultimate Stress | 261 ksi |
| Material: | AS1/3501-6 |
| Test Rate | 0.05 in/min |
| Environment | Ambient |
| Initial Defects | None |
| Failure Sequence | Catastrophic |

Primary Failure Surface Characteristics

| Figure | Characteristic |
|---|---|
| a | Irregular contour (macroscopic) |
| b | Blunted Spires |
| b | Diagonally fractured fibers |

Figure 27a Macroscopic View of $0^0$ Tensile Specimen, 2.5X

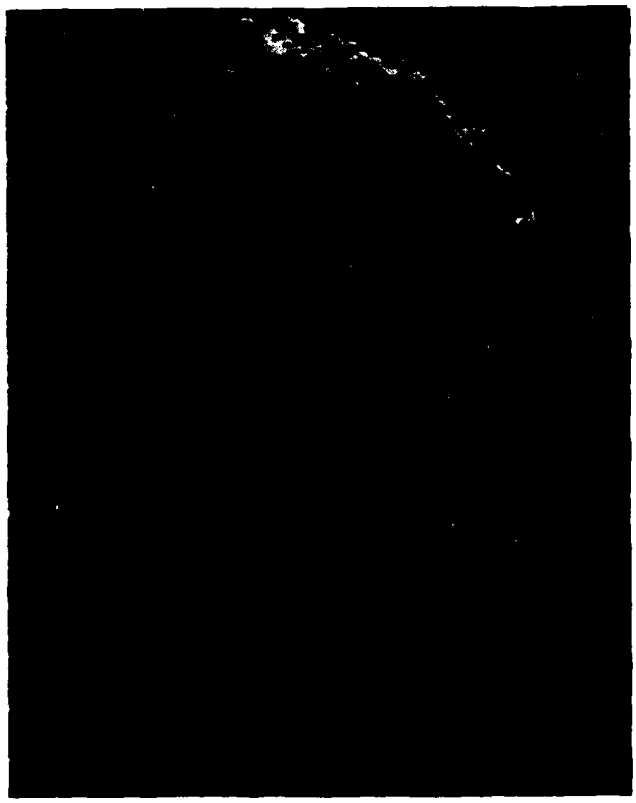

Figure 27b Photomicrograph of $0^0$ Tensile Specimen, 200X

Figure 28 ±45 Tension

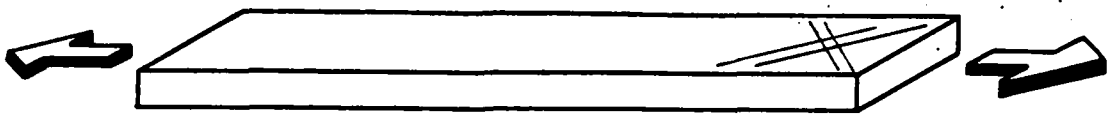

| | |
|---|---|
| Specimen: | T45 - A21 |
| Stress State | $\tau_{12}$ Complex |
| Ultimate Stress | 24.6 ksi |
| Average (of 5) | |
| Ultimate Stress | 25.4 ksi |
| Material: | AS1/3501-6 |
| Test Rate | 0.01 in/min |
| Environment | Ambient |
| Initial Defects | None |
| Failure Sequence | $45^{o}$ ply-cracking, ply delamination, Failure (see Figures a and b) |

Primary Failure Surface Characteristics

| Figure | Characteristic |
|---|---|
| a | Plan view of Failed specimen (macroscopic) |
| b | Edge view of Failed specimen (macroscopic) |
| c | Tensile failure mode |
| d,e | Fiber failure |
| e | Delaminations |
| f | Debris |

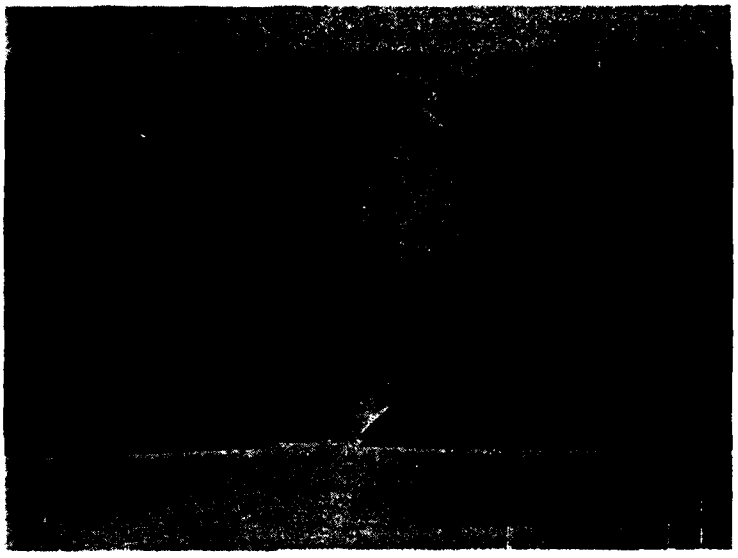

Figure 28a Macroscopic Plan View of Broken ±45° Specimen, 2X

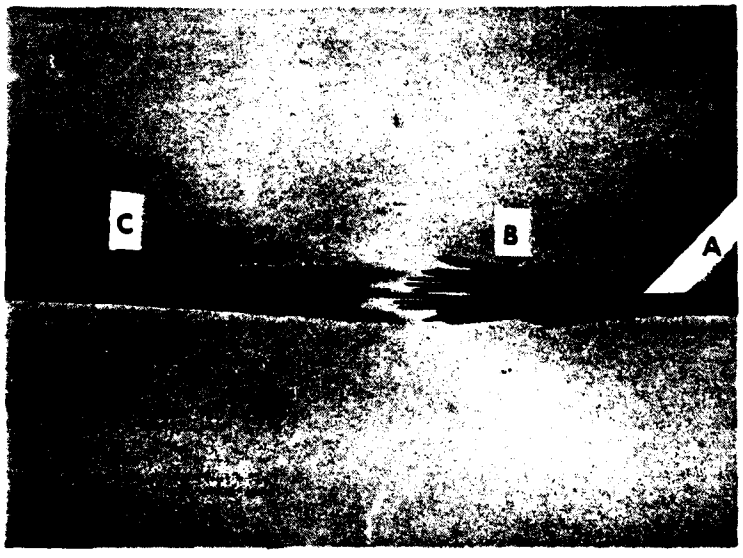


Figure 28b Macroscopic Edge View of Broken ±45° Specimen, 2X

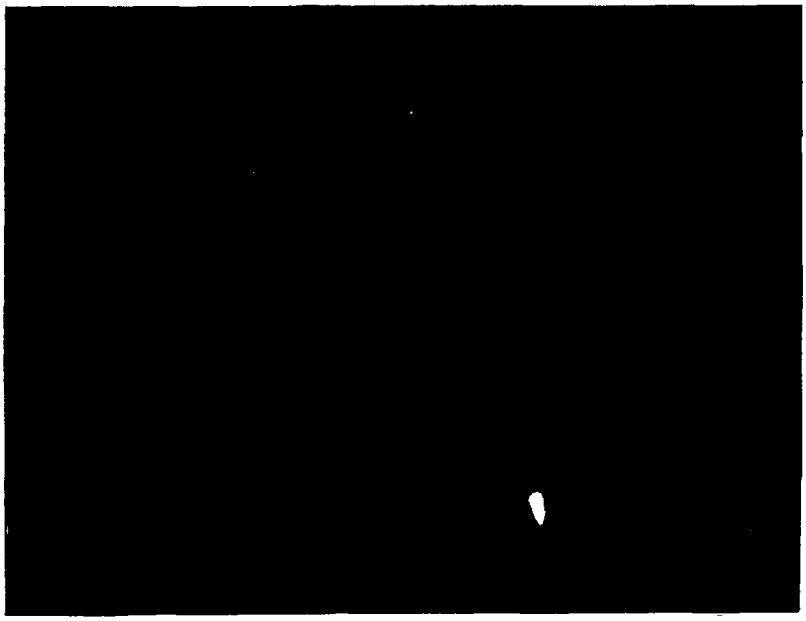

Figure 28c Plane of Transverse Crack in +45° Specimen , 1000X

Figure 28d Broken Fibers in ±45° Specimen, 1000X

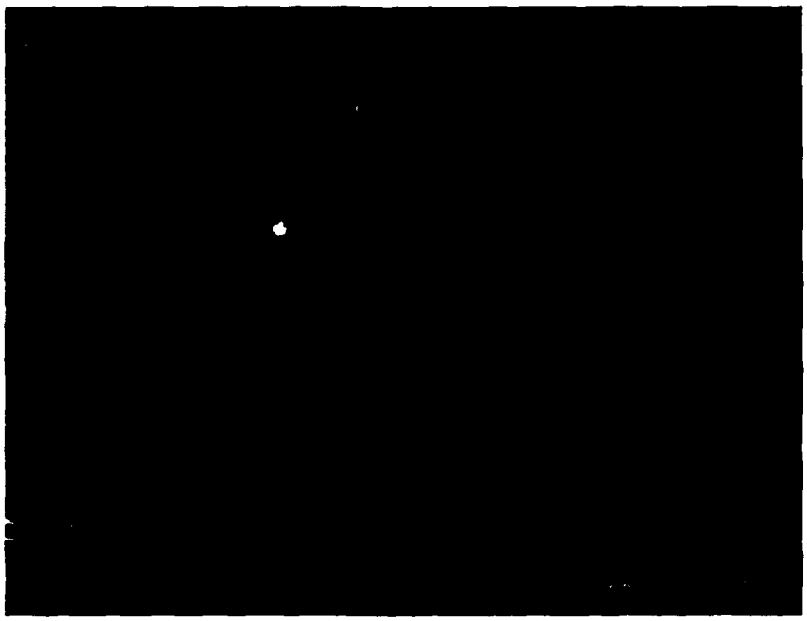

Figure 28e Fiber Breakage & Delaminations of Intersections of Transverse Cracks in $\pm 45^0$ Specimen, 100X

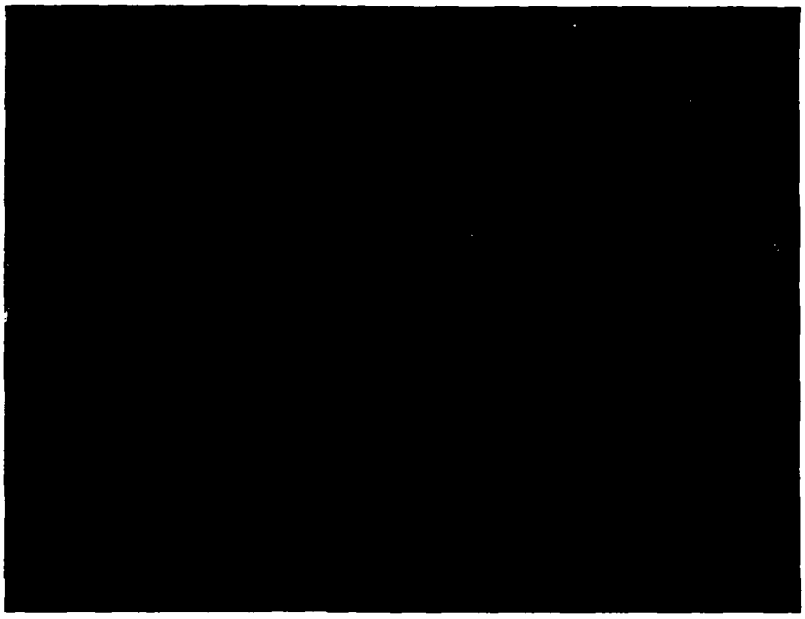

Figure 28f Debris Characterizing the Location of Final Catatrophic Failure in $\pm 45^0$ Specimen, 1000X

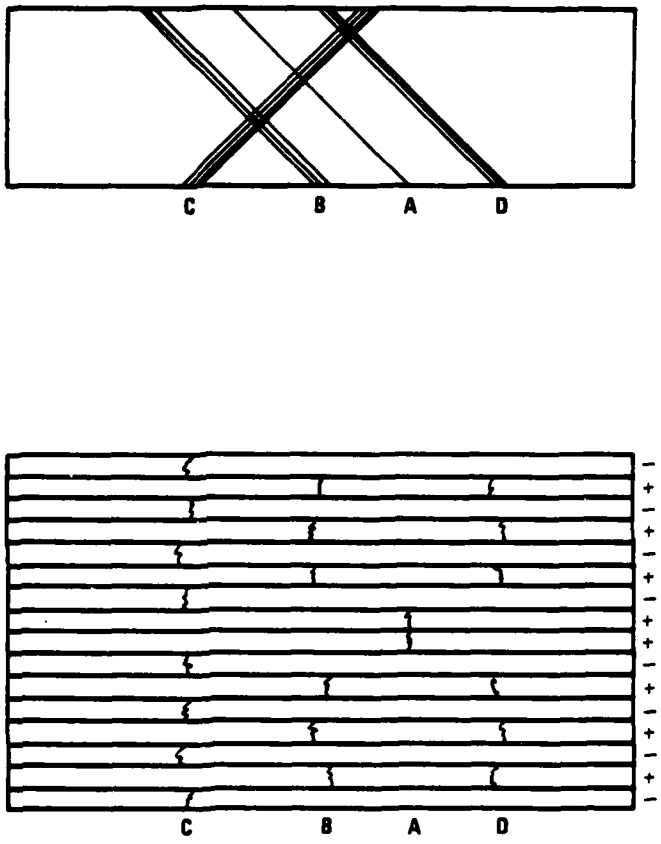


**Figure 29 Schematic of Transverse Cracks in ±45° Specimen**

of cracks in the +45° plies (B and D in Fig. 29) were equidistant from the transverse crack in the two central +45° laminae. The corresponding locations of the bands of the transverse cracks are identified in Figures 28b (photograph) and 29 (schematic) although band D is not within the field of view of Figure 28b. A view of the plane of a transverse crack is shown in Figure 28c and is indicative of primarily tensile failure. Localized fiber breakage occurs in the +45° laminae in areas where transverse cracks in the -45° plies (band C) intersect, in plan view, the transverse cracks in the +45° plies (bands B and D and crack A in Fig. 29). The failure surface of these fibers is shown in Figure 28d and has the same appearance as that of 0° fibers in tension. The localized fiber breaks at the intersections of transverse cracks are shown in Figure 28e and are the initiators of delaminations which are also shown there. The delaminations grow until massive fiber failure occurs in the +45° laminae across the width of the specimen as depicted by the central area of Figure 28a. The final, catastrophic failure site is characterized by a considerable amount of debris (Fig. 28f).

Tension-tension fatigue testing was conducted on 90° and ±45° laminae and $[0/\pm45/90]_{2S}$ laminates. On a microscopic scale,it was found that the fractographic features of the 90° laminae were the same as in the case of monotonic tension. Macroscopic observations of the ±45° laminae and the quasi-isotropic laminates led to the same conclusion and microscopy was not therefore undertaken.

## 4.6 Compression Specimens

### 4.6.1 90° Laminae

On a macroscopic scale, the 90° compression specimens fail due to the formation of two major fracture planes which intersect in the form of an "X". These planes occur approximately along the line of maximum shearing stresses (±45°). Figure 30a is a photograph of the edge of a specimen and shows that, on the right half of the specimen, an apex is formed by the intersecting planes. A view of the apex feature in the same specimen is shown in Figure 30b which also indicates that a small number of plies at the surface form a planar shelf which is roughly perpendicular to the direction of loading. A 50X magnification of the apex area shown in Figure 30b is shown in Figure 30c. The face to the left side of the specimen (left) has a noticeable lack of debris when compared to the face on the

Figure 30 $90^{\circ}$ Compression

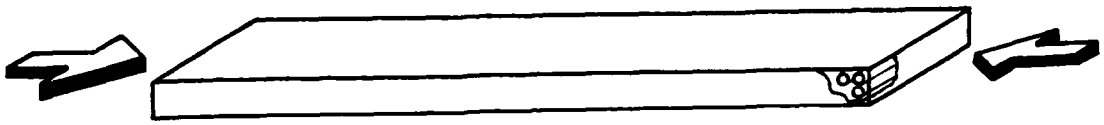

| | |
|---|---|
| Specimen: | C90 - A4 |
| Stress State | $\sigma_{22}$ (Compression) |
| Ultimate Stress | 23.0 ksi |
| Average (of 2) | |
| Ultimate Stress | 20.9 ksi |
| Material: | AS1/3501-6 |
| Test Rate | 0.05 in/min |
| Environment | Ambient |
| Initial Defects | None |
| Failure Sequence | Catastrophic |

Primary Failure Surface Characteristics

| Figure | Characteristic |
|---|---|
| a | "X" - mode feature (macroscopic) |
| b | Apex (macroscopic) |
| c | Apex |
| d | Debris due to abrasion |
| e | River markings |
| f,g | Hackles |
| g | Crack propagating inward |
| h | Mode I - Mode II Transition |

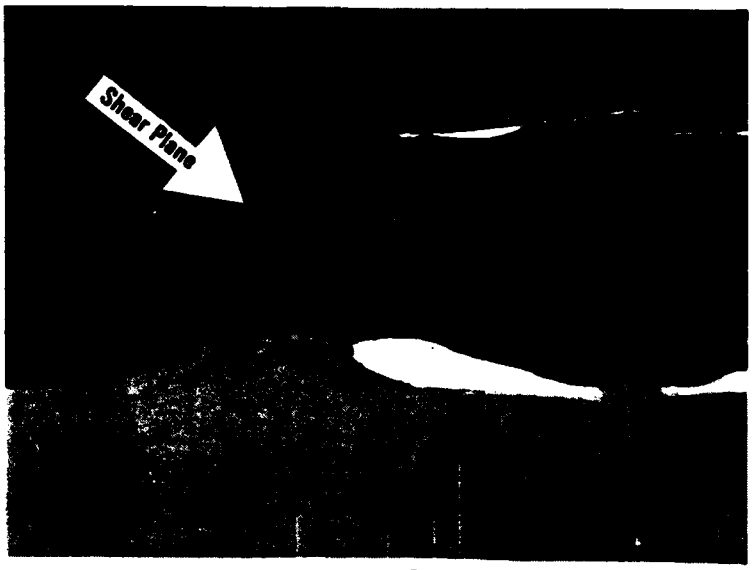


Figure 30a "X" Mode of Failure in 90° Specimens Under Compression , 5X

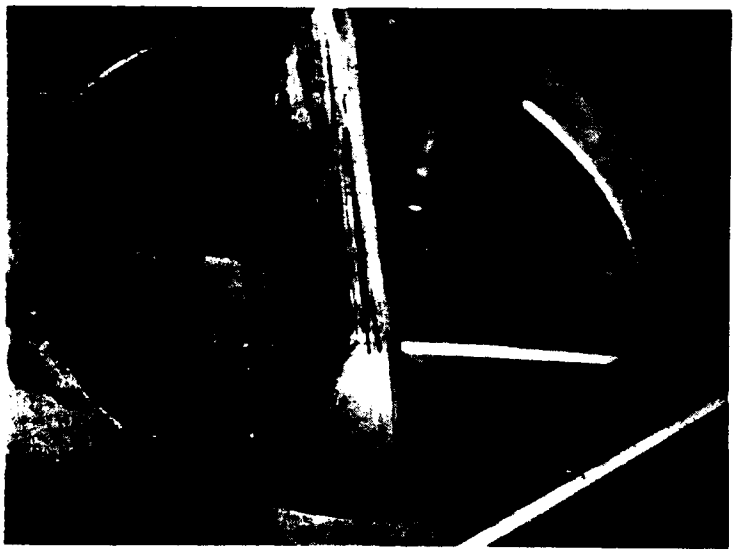

Figure 30b Apex Feature in 90° Specimens Under Compression , 2X

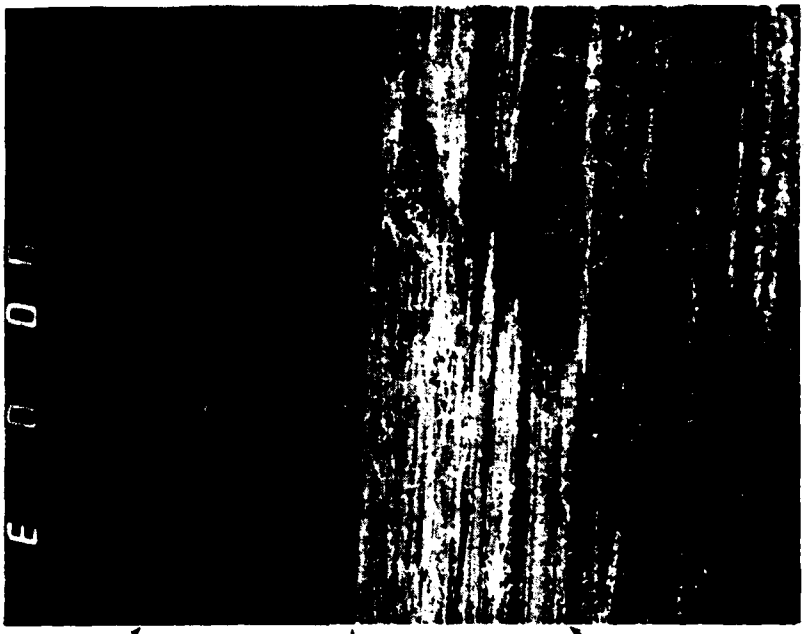

DEBRIS FREE SIDE APEX GRANULATED SIDE

Figure 30c Tensile & Compressive Faces of Apex Feature , 50X

Figure 30d Debris Formed by Abrasion on Compressive Face of Apex Feature , 1500X

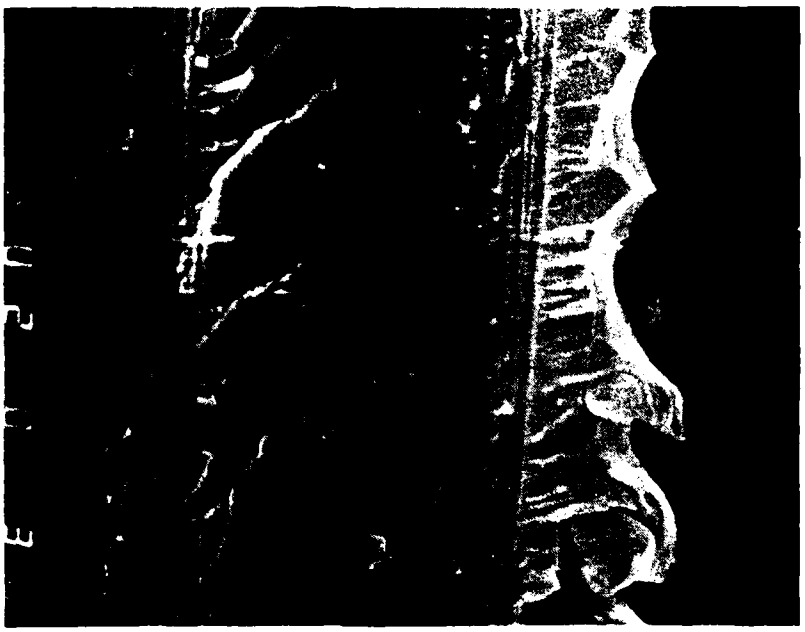

Figure 30e River Markings on Debris Free of Apex Feature , 5000X

Figure 30f Hackles on 90° Fracture Surface, 5000x

Figure 30g Edge View of Transverse Crack, 1500x

Figure 30h Mode I – Mode II Transition, 1500x

compressive side. Figure 30d shows a photomicrograph of the granulation believed to have been formed by abrasion between the surfaces. Consequently, the features of the fracture surface were obliterated by secondary damage formations. Consequently, emphasis was placed upon the right side where the features remained free of debris. In Figure 30e (5000X), the apex is to the right and the tensile face is to the left. The cleavage planes are relatively smooth and the river markings imply that the crack direction was from left to right (i.e., originated at the edge and propagated toward the apex). Evidence of shear failure is also evident on this surface. Figures 30f,g are an example of the hackle patterns typical of shear failure. Also in Figure 30g a crack extending into the surface is evident. In summation, this failure surface is mixed mode, evidence of both Mode I and II are found. Figure 30h is an example of a transition region between Mode I left and Mode II right.

### 4.6.2 ±45° Laminae

Three major features that were observed on a macroscopic scale in the ±45° compression specimens were slip steps in the lamina planes, kinking perpendicular to the lamina planes and delamination at the interfaces. Figure 31a indicates bulges in the mid-section of the specimen which are due to slipping along the +45° and -45° fiber directions. The kinking is shown in an edge view in Figure 31b which also indicates the presence of some delaminations.

Figure 31c is a 10X magnification of the edge of a specimen. It clearly defines the slipping, kinking and delamination features. The slipping is marked by the transverse cracks and the steps of material which have been pushed out between one crack to another. Notice also that, on this edge of the specimen, the outward slippage and matrix occurs in every second lamina. Matrix cracks are visible in the in-between laminae although inward slippage cannot be discerned. However, observation of the other edge of the specimen indicates that the in-between laminae are indeed pushed out of that edge. The direction of slip is therefore governed by the orientation of the plies and its cumulative effect gives rise to bulging on both sides of the specimen that was pointed out in Figure 31a. Figures 31d and 31e are 100X and 500X magnifications of the center plies in the kinked region. They indicate that very few fiber fractures occur (Fig. 31e) and that fracture is confined to the resin in the form of matrix cracks and delaminations.

Figure 31 $\pm 45^{\circ}$ Compression

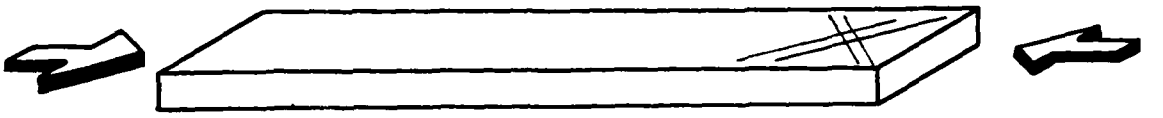

| | |
|---|---|
| Specimen: | A45-4 |
| Stress State | $\tau_{12}$ complex |
| Ultimate Stress | 29.6 ksi |
| Average (of 2) | |
| Ultimate Stress | 30.2 ksi |
| Material: | AS1/3501-6 |
| Test Rate | 0.05 in/min |
| Environment | Ambient |
| Initial Defects | None |
| Failure Sequence | Instability, kinking, ply cracking, delamination, failure. |

Primary Failure Surface Characteristics

| Figure | Characteristic |
|---|---|
| a | Bulging (macroscopic) |
| b,c,d | Kinking, slip and delamination |
| e | Unbroken fibers along failure surface |
| f | Mode I and Mode II Features |

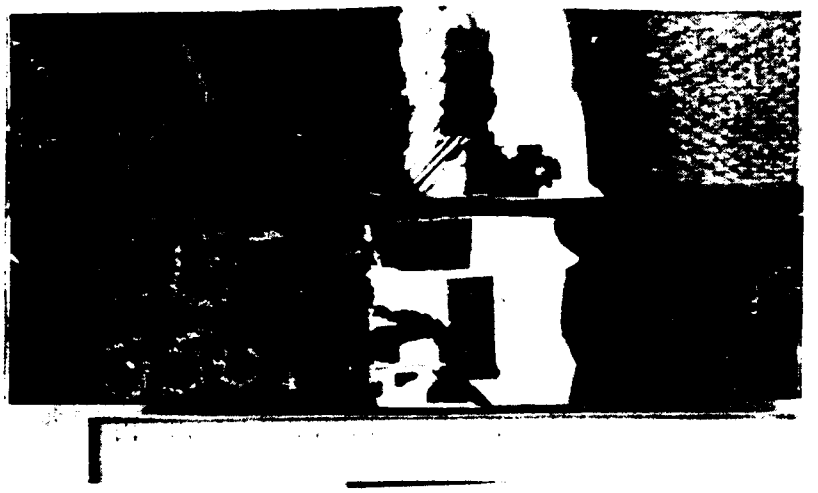

Figure 31a Macroscopic View of Bulging of $\pm 45^{0}$ Specimens in Compression, 1X

Figure 31b Kinking in $\pm 45^{0}$ Specimens in Compression, 5X

Figure 31c Kinking, Slip & Delaminations in $\pm 45^0$ Specimens in Compression, 10X

Figure 31d Higher Magnification of Kinking, Slip & Delaminations in $\pm 45^0$ Specimens in Compression, 100X

Figure 31e Unbroken Fibers in ±45° Specimens in Compression, 500X

Figure 31f Mixture of Mode I & Mode II Features in ±45° Laminae Under Compression, 2000X

At 2000X magnification (Figure 31f), a mixture of Mode I and Mode II features are evident.

### 4.6.3 Quasi-Isotropic Laminate

A composite photograph of the edge of a broken quasi-isotropic laminate and taken at 5X magnification is shown in Fig. 32. Fiber fracture occurs along two offset transverse planes, originating from either face of the specimen. In the regions away from these planes, 0° plies are still intact. There are many intraply delaminations in the ±45° and 90° laminae. Interply delaminations are numerous within the area bounded by the regions of transverse fracture and gradually diminish towards the ends of the specimens.

## 4.7 Impact Damage Specimen

The fractographic investigation was conducted on a 28-ply thick panel made of T300/5208 and whose stacking sequence is identified in Figure 33b. In Figures 33a,b the impact occurred at the face to the bottom of the photograph with the backface being at the top. There is extensive interply delamination throughout the laminate thickness. Transverse cracking occurs in all the +45° and 0° plies. Some of the transverse cracks are oriented at -45° to the direction of impact in a truncated cone pattern, which may be indicative of shear failure. There is considerable backface damage due to the tensile nature of the reflected impact wave.

Figure 32 Quasi-Isotropic Compression

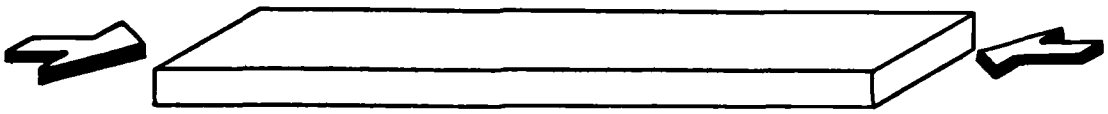

| | |
|---|---|
| Specimen: | TQI-2 |
| Stress State | Complex |
| Ultimate Stress | 76.4 ksi |
| Average (of 2) | |
| Ultimate Stress | 79.6 ksi |
| Material: | T300/5208 |
| Test Rate | 0.05 in/min |
| Environment | Ambient |
| Initial Defects | None |
| Failure Sequence | Instability, ply cracking, kinking, delamination, failure |

Primary Failure Surface Characteristics

| Figure | Characteristic |
|---|---|
| a | Fiber fracture, delamination |
| a | Transverse plane |

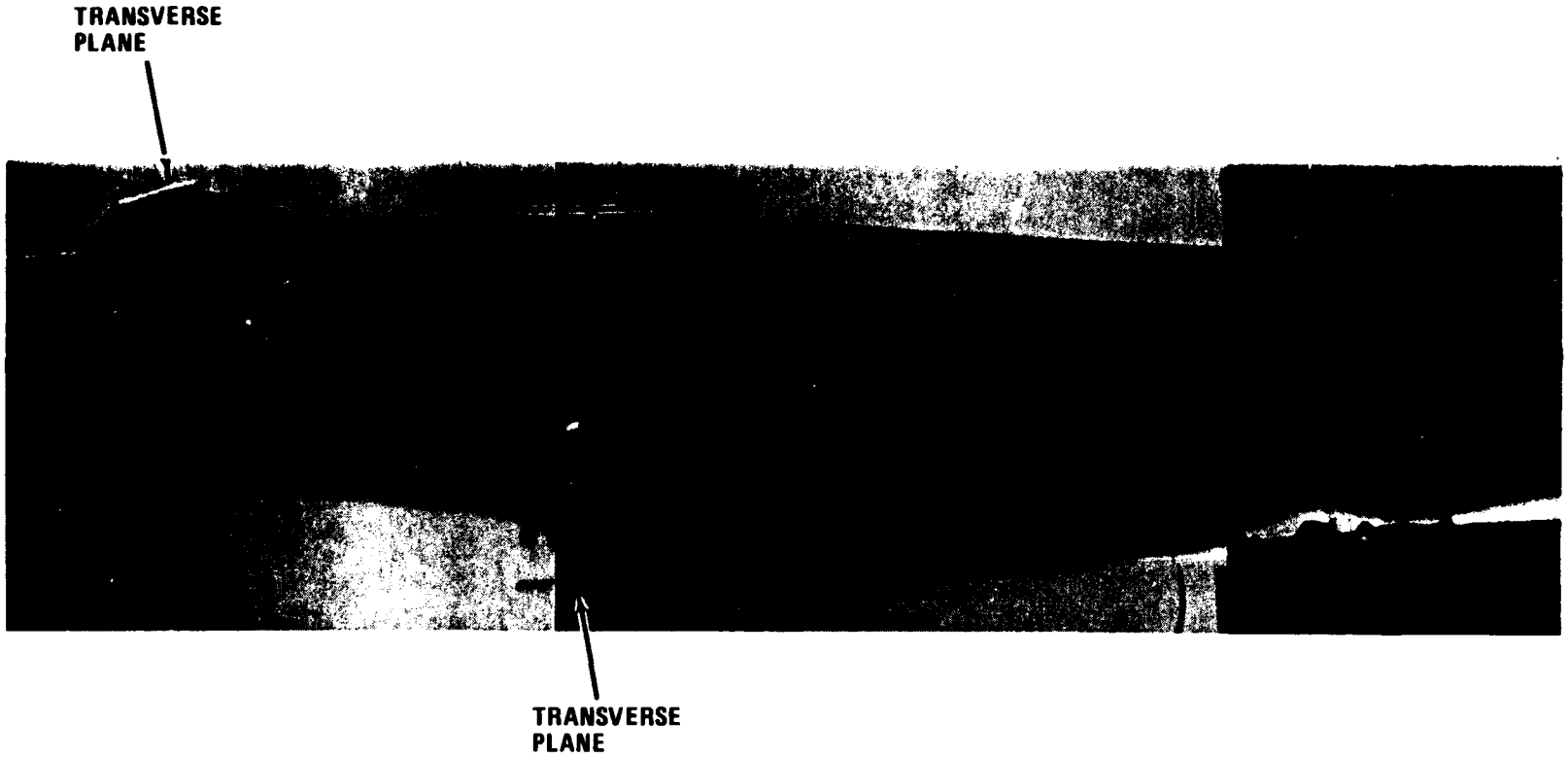


Figure 32 Compressive Failure of Quasi-Isotropic Laminate , 5X

Figure 33 Transverse Impact

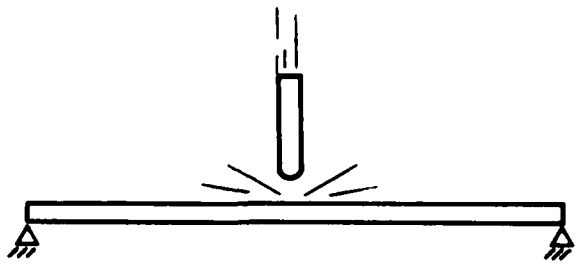

| | |
|---|---|
| **Specimen:** | 811-C2L2 |
| **Stress State** | Complex |
| Impact Energy | 6.8 ft-lbs |
| Absorbed Energy | 4.1 ft-lbs |
| Damaged Area | 1.4 $in^2$ |
| **Material:** | T300/5208 |
| Stacking Sequence | $[\pm 45/+45/90/-45(\pm 45/0)_2/\pm 45/\overline{\pm 45}]_S$ |
| **Environment** | Ambient |
| **Initial Defects** | None |
| **Failure Sequence** | Unknown, but expect transverse cracks to occur first, followed by delamination |

**Primary Failure Surface Characteristics**

| **Figure** | **Characteristic** |
|---|---|
| a,b | Transverse cracking and delamination |

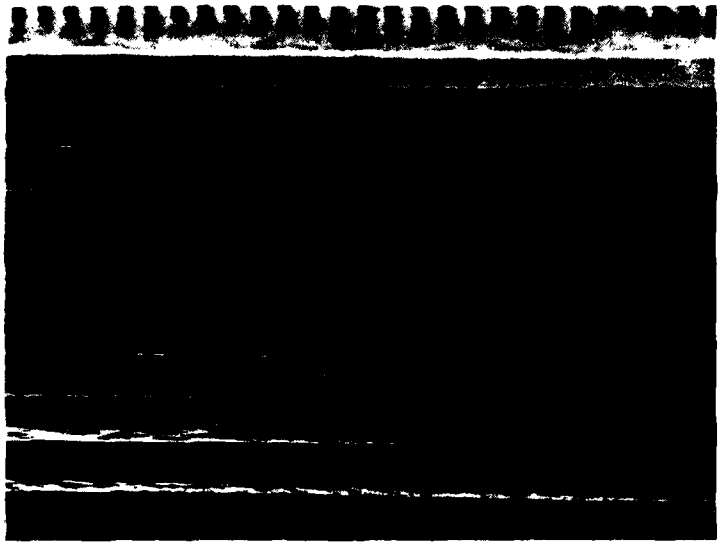

Figure 33a Transverse Cracking & Delaminations in Impact Specimen , 20X

Figure 33b Higher Magnification of Transverse Cracking & Delamination in Impact Specimen , 35X

## 5. CONCLUDING REMARKS

Fractography has been performed on a variety of basic graphite epoxy specimens which were subject to a number of fundamental loading modes. The results indicate that the fracture of composite materials is controlled by local conditions; i.e., local fiber-matrix interactions. As a result, there are many local fractographic features which are often apparently contradictory in their interpretation. The material inhomogeneities which are a part of composite materials can cause a number of crack initiation sites. Interpretation of failure is further complicated by the large degree of fragmentation that occurs at failure.

Nonetheless, features have been identified which are representative of global material response. In general, the matrix material rather than the fibers has been found to contain the fractographic elements which are most useful in interpreting the global behavior of the component under investigation. The fractographic features most commonly found in the matrix material are hackles, river patterns and feather patterns. They were repeatedly observed throughout the failure surfaces of individual specimens and appear to be formed by brittle fracture processes. They are, however, not unique to any one individual loading mode. Furthermore, the existence of any one feature will not necessarily totally define a failure mode. These features are necessary but not sufficient to determine a general material failure condition. For example, hackle patterns were found not only in the Arcan shear specimen and the Mode II fracture specimens (not surprising since the same basic loading was involved in both specimens) but also in the 90° tensile specimens. The mechanisms contributing to these three basic fractographic features of the matrix material are now discussed.

It is recognized that the matrix material is viscoelastic and that the response of the matrix material cannot always be assumed to be brittle. However, at the dry, room temperature and relatively high loading rate conditions under which the testing of the specimens was conducted, the matrix material is essentially brittle. The appearances of the three basic fractographic features can therefore be accounted for by applying the concepts of brittle fracture.

The fracture plane in any loading condition in a brittle material is perpendicular to the maximum resolved tensile direction (Fig. 34a). When the fibers lie perpendicular to

T – MAXIMUM PRINCIPAL STRESS DIRECTION

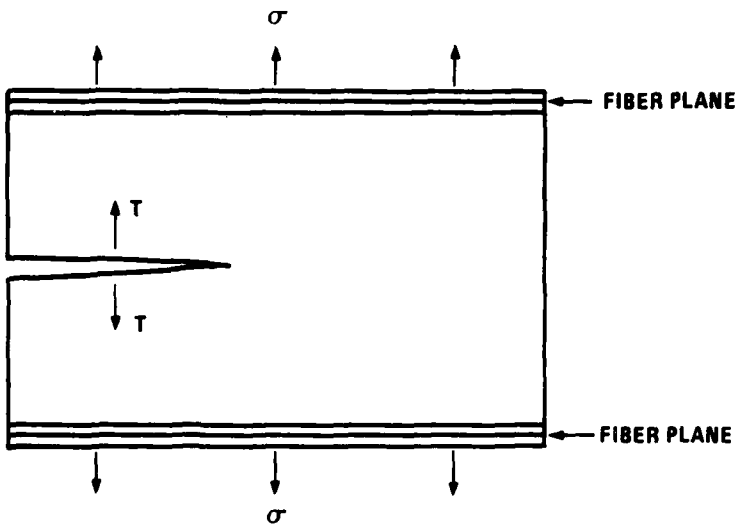


(A) LOCAL TENSILE STRESS FIELD

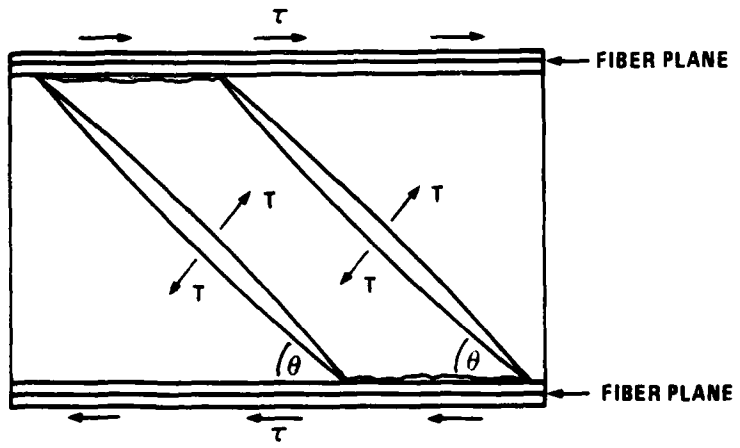


(B) LOCAL SHEAR STRESS FIELD

Figure 34 Schematic of Formation of Cleavage and Hackle Features

the maximum tensile direction, a single cleavage plane parallel to the fibers results. The features of river and feather patterns fall into this category. However, when the fibers are not perpendicular to the maximum tensile direction, e.g., in a situation where shear is locally predominant, the fracture plane intersects the plane of the fibers. The fiber planes generally restrict any further growth of the crack with the result that a series of parallel fissures occur in the region between the fiber planes (Fig. 34b). Such conditions give rise to the hackle feature, which has also been observed in the analogous situation of a metal-to-metal adhesively bonded joint loaded in shear. The occurrence of all three features on some occasions indicates that the local stress state should be considered in conjunction with the globally applied loading in the inspection of any failure surface.

AD-A125 832 SEM/TEM FRACTOGRAPHY OF COMPOSITE MATERIALS(U) GENERAL DYNAMICS FORT WORTH TX FORT WORTH DIV K M LIECHTI ET AL. SEP 82 AFWAL-TR-82-4085 2/2

UNCLASSIFIED F33615-79-C-5121 F/G 11/4 NL

END
DATE
FILMED
4 83
DTIC

M-2

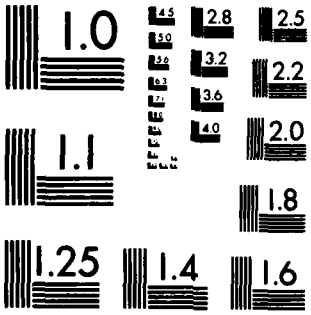


MICROCOPY RESOLUTION TEST CHART
NATIONAL BUREAU OF STANDARDS-1963-A

## REFERENCES


1. American Society for Metals, 8th Edition, Vol. 9, "Fractography and Atlas of Fractographs," 1974.

2. Jones, R. M., Mechanics of Composites Materials, Washington, D.C., Scripta Book Co., 1975.

3. Miller, A. G. and Wingert, A. L., "Fracture Surface Characterization of Commercial Graphite/Epoxy Systems," Nondestructive Evaluation and Flaw Criticality For Composite Materials, ASTM STP 696, R. B. Pipes, Ed., American Society for Testing and Materials, 1979, pp. 223-273.

4. Clements, L. L. and Lee, P. R., "Influence of Quality Control Variables on Failure of Graphite/Epoxy Under Extreme Moisture Conditions," NASA Technical Memorandum 81246, October 1980.

5. Clements, L. L. and Adamson, M. J., "Failure Morphology of Graphite/Epoxy As Influenced by Environments and Processing," presented at ASTM's Sixth Conference on Composite Materials: Testing and Design, May 12-13, 1981, Pheonix, AZ.

6. Chamis, C. C. and Sinclair, J. H., "Mechanical Behavior and Fracture Characteristics of Off-Axis Fiber Composites. I - Experimental Investigation," NASA Technical Paper 1081, 1977.

7. Chamis, C. C. and Sinclair, J. H., "Mechanical Behavior and Fracture Characteristics of Off-Axis Fiber Composites. II - Theory and Comparisons," NASA Technical Paper 1082, 1978.

8. Awerbuch, J. and Hahn, H. T., "Off-Axis Fatigue of Graphite/Epoxy composite," Fatigue of Fiberous Composite Materials, ASTM STP 723, American Society for Testing and Materials, 1981, pp. 243-273.

9. Morris, G. E., "Determining Fracture Directions and Fracture Origins on Failed Graphite/Epoxy Surfaces," Nondestructive Evaluation and Flaw Criticality For Composite Materials, ASTM STP 696, R. B. Pipes, Ed. American Society for Testing and Materials, 1979, pp. 174-297.

10. Adams, D. F., "Compression Fatigue and Fracture Modes in Graphite/Epoxy Laminates," Proceedings of the ASME Winter Annual Meeting, "Advances in Aerospace Structures and Materials - I," Washington, D.C., November 1981.

11. Adams, D. F., "Investigation of Compression Fatigue Properties of Advanced Composites," Final Technical Report, Oct. 1979, Naval Air System Command Contract No. N00019-77-C-5019.

12. Morris, G. E., and Hetter, C. M., "Fractographic Studies of Graphite/Epoxy Fatigue Specimens," Damage in Composite Materials, ASTM STP 775, American Society for Testing and Materials, 1982.

13. Adams, D. F. and Perry, J. L., "Static and Impact Behavior of Graphite/Epoxy Composite Laminates Containing Third-Phase Reinforcement Materials," Journal of Testing and Evaluation, JTEVA, Vol. 5, No. 2, March 1977, pp. 114-123.

14. Adams, Donald F., "A Scanning Electron Microscopic Study of Hybrid Composite Impact Response," Journal of Material Science, Vol. 10, 1975, p. 1591-1602.

15. Purslow, D., "Some Fundamental Aspects of Composites Fractography," Composites, October 1981, pp. 241-247.

16. Carpenter, J. F., "Test Program Evaluation of Hercules 3501-6 Resin," Final Technical Report, May 1978, Naval Air Systems Command Contract No. N00019-77-C-0155.

17. Kibler, K. G., "Time Dependent Environmental Behavior of Graphite/Epoxy Composites," Final Technical Report, May 1980, Air Force Materials Laboratory AFWAL-TR-80-4052.

18. Eisenmann, J. R., et al. "Analysis Methods Development for Advanced Composites; Strength, Durability and Damage Tolerance," General Dynamics Report ERR-FW-2124, 1980.

19. Wilkins, D. J. et al. "Characterizing Delamination Growth in Graphite/Epoxy," ASTM STP 775, American Society for Testing and Materials, 1982.

20. General Dynamics Fort Worth Division FPS 2003, #B-001.

21. Conrad, E. G., "Composite Impact Damage Evaluation," General Dynamics Report ERR-FW-2128, Dec. 1980.

22. Conrad, E. G., "Composite Panel Impact Damage," General Dynamics Report ERR-FW-2206, July 1981.

23. Semi-annual Progress Report No. 1 (23 February to 23 September 1981), "Cumulative Damage Model for Advanced Composite Materials," Fort Worth Division Technical Report FZM 7021, December 1981.

APPENDIX

## COMPOSITE MATERIAL FRACTOGRAPHY RECORD

INVESTIGATOR

Date

A. SPECIMEN INFORMATION

(1) Constituent Material/Materials

Fiber

Matrix

(2) Laminate

Size and Shape

Stacking Sequence

Number of Plies

Fiber Volume Fraction

Matrix Volume Fraction

Type of Fabrication Process

B. LOADING INFORMATION

(1) Type of Test

(2) Test Conditions

Temperature

Humidity

(3) Orientation of Laminate Principal Axis to Loading Direction (Attach Sketch)

C. SCANNING ELECTRON MICROSCOPE INFORMATION

(1) Specimen Preparation

Coating

Special Prep.

(2) Viewing Conditions

Viewing Mode

Accelerating Voltage (kv)

Specimen Tilt ($^{o}$)

Sem Image Enhancement

Special Conditions

D. FRACTOGRAPHY INFORMATION

Failure Mode

Fracture Plane (Attach Sketch)

Features

Description of Features and their Chronology (Attach Photomicrograph)

Magnification

Other



*USGPO: 1983 659-062-786